www.acsnano.org

Simultaneous and Multimodal Antigen-Binding Profiling and Isolation of Rare Cells via Quantitative Ferrohydrodynamic Cell Separation

Yang Liu,* Rafaela Maggioni Simoes Vieira, and Leidong Mao*



Downloaded via GEORGIA INST OF TECHNOLOGY on July 11, 2024 at 13:25:55 (UTC). See https://pubs.acs.org/sharingguidelines for options on how to legitimately share published articles.

Cite This: ACS Nano 2023, 17, 94-110



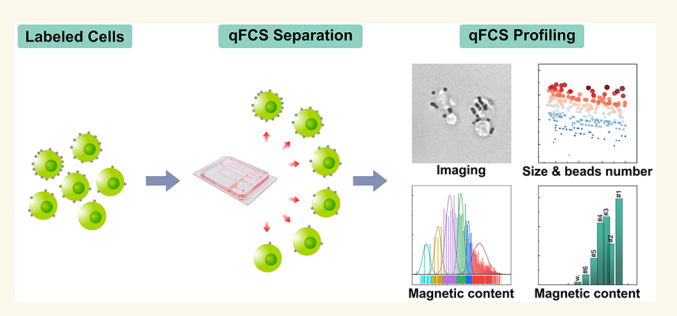
ACCESS I

III Metrics & More

Article Recommendations

Supporting Information

ABSTRACT: Simultaneous cell profiling and isolation based on cellular antigen-binding capacity plays an important role in understanding and treating diseases. However, fluorescence-activated cell sorting (FACS) and magnetic-activated cell sorting (MACS) are not able to meet this need, due to their requirement for a large quantity of target cells and the limitation stemming from bimodal separation. Here we report a microfluidic method, termed quantitative ferrohydrodynamic cell separation (qFCS), that achieved multimodal rare cell sorting and simultaneous antigen profiling at a ~30,000 cell min⁻¹ throughput with a 96.49% recovery rate and a 98.72%



purity of recovered cells. qFCS profiles and sorts cells via cellular magnetic content of the magnetically labeled cells, which correlates to cellular antigen-binding capacity. By integrating cellular magnetophoresis and diamagnetophoresis in biocompatible ferrofluids, we demonstrate that the resulting qFCS device can accurately profile and isolate rare cells even when present at ~1:50,000 target to background cells frequency. We show that the qFCS device could accurately profile and isolate T lymphocytes based on a low-expression CD154 antigen and allow on-device analysis of cells after processing. This method could address the need for simultaneous and multimodal rare cell isolation and profiling in disease diagnostics, prognostics, and treatment.

KEYWORDS: cell separation, antigen-binding profiling, antigen-based separation, ferrohydrodynamic cell separation, rare cell separation, ferrofluid

rofiling of surface antigen expression on rare cells and their isolation for subsequent functional, protein, and genetic analyses in a biological sample have significant implications in disease diagnostics, prognostics, and treatment.¹⁻⁴ For example, in human immune-mediated diseases, rare immune cells collected from patients were separated and analyzed according to their antigens to evaluate the immune function, disease state, and therapeutic effects. 5-7 In human cancers, rare circulating tumor cells in the blood circulation of the patients were sorted and characterized based on their antigens to understand metastasis and inform therapeutic options.8-13 Surface antigen molecules on the rare cells are responsible for a wide range of cellular functions, and their expressions are often heterogeneous and can evolve dynamically over the course of the cell cycle, making simultaneous antigen-based profiling and cell isolation a critical but challenging task. This task is further compounded by the rarity of the target cells, which can occur when they exist at

very low frequencies in a complex matrix or when a limited amount of samples is available. These challenges made it difficult for the application of conventional methods to accomplish antigen profiling and cell isolation at the same time. Even though fluorescence-activated cell sorting (FACS) has been well established for antigen profiling, it has limited success in rare cell applications, and cells profiled by FACS are not always suitable for subsequent analyses. An alternative magnetic-activated cell sorting (MACS) can isolate rare cells from a sample for downstream analysis via magnetic labeling of

Received: May 9, 2022
Accepted: December 19, 2022
Published: December 21, 2022





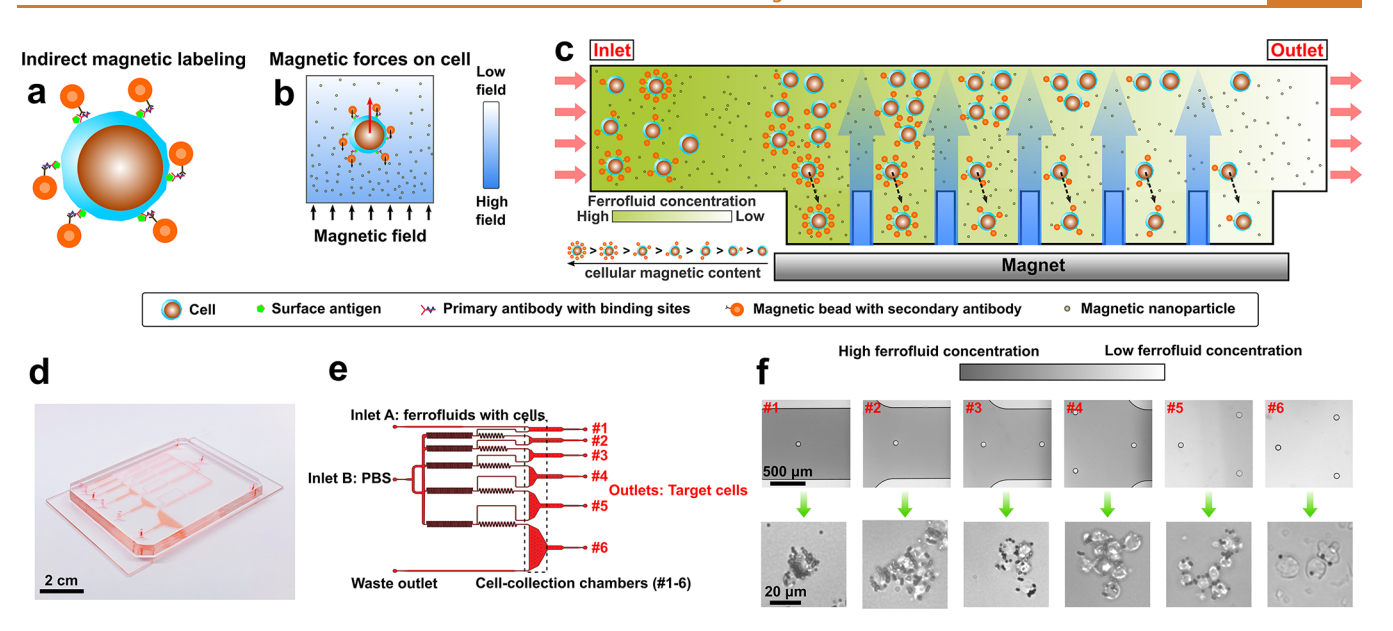


Figure 1. Overview of the quantitative ferrohydrodynamic cell separation (qFCS) method and its prototype device. (a) Schematic of indirect magnetic labeling in which a primary antibody binds against a specific cell surface antigen, a secondary antibody conjugated to a magnetic bead, then binds to the primary antibody through secondary binding sites. In this process, the cellular magnetic content of the cell-beads complex becomes proportional to the cell's antigen-binding capacity (the number of primary antibodies bound to the cell surface) under specific conditions. (b) Schematic of a cell-beads complex experiencing competing "magnetophoresis" and "diamagnetophoresis" in ferrofluids, which is a colloidal suspension of magnetic nanoparticles. Magnetophoretic force on the cell-beads complex results from the conjugated magnetic beads and directs the cell-beads complex toward the maximum of a nonuniform magnetic field (black arrows). Diamagnetophoretic force on the cell-beads complex results from magnetic nanoparticle-induced pressure imbalance on the cell-beads complex's surface and directs it toward the minima of the magnetic field (red arrow). These two magnetic forces are in opposite directions. Color bar indicates the gradient of the magnetic field. (c) Schematic of the qFCS device design. Cell-beads complexes continuously flow through six stages of the ferrofluids in the qFCS. When the condition $\phi_{\text{cell-beads}} \leq \phi_{\text{ferrofluid}}$ is met, diamagnetophoretic force on the cell-bead complex equals or overcomes the magnetophoretic force and drives it to the next stage. When the condition $\phi_{\text{cell-beads}} > \phi_{\text{ferrofluid}}$ is met, the magnetophoretic force outweighs the diamagnetophoretic force and traps the cell-beads complex in the current stage. Each stage of the qFCS with a ferrofluid concentration $\phi_{\text{ferrofluid} \otimes^{\#_n}}(n \text{ is } n^{\text{th}} \text{ stage})$ can trap cell-beads complexes with their cellular magnetic contents falling in the range of $\phi_{\text{ferrofluid}@\#n-1} \ge \phi_{\text{cell-beads}} > \phi_{\text{ferrofluid}@\#n}$, which is proportional to the cell's surface antigen-binding capacity α , resulting in cell isolation based on the levels of antigen-binding capacity. At the same time, distributions of a specific antigen-binding capacity among the cell population can be profiled in qFCS by counting the cell-beads complexes in each stage. Blue arrows indicate the gradient of the magnetic field. Green coloring in the device indicates the gradient of the ferrofluid concentration. (d) A photo of the microfluidic channels in the qFCS device. (e) Top view of the qFCS microchannels. Cells suspended in the ferrofluid are injected into inlet A, and PBS buffer from inlet B is applied to mix with the ferrofluid for dilution and generate spatially stable and variable concentrations in qFCS stages and cell-collection chambers #1-6. (f) (Top panel) Ferrofluid concentration decreases continuously from stages and cell-collection chambers #1-6 in the qFCS device. (Bottom panel) Experimental images of the qFCS device in the isolation of white blood cells (WBCs) labeled with CD45modified magnetic beads. As the ferrofluid concentration decreases from stage #1 to #6, the number of microbeads on WBCs and the corresponding cellular magnetic contents also decrease.

surface antigens; however, it lacks the ability to perform multimodal isolation based on the quantitative levels of antigen expressions, due to the fact that it operates primarily via a bimodal separation mechanism.¹⁵ Because of the limitations facing the conventional methods, it is urgently needed to profile surface antigens from limited amounts of biological cells and isolate the cells based on their antigen expressions in a multimodal manner.

We report a microfluidic method that performs simultaneous and multimodal rare cell profiling and isolation based on a cellular property—cellular magnetic content—which is shown to correlate to a magnetically labeled cell's antigen-binding capacity. This method relies on a microfluidic device architecture that achieves precise control over the concentration of a magnetic medium (ferrofluids) along a microchannel, resulting in concurrent characterization and isolation of magnetically labeled rare cells according to their magnetic contents and antigen-binding capacities with single-cell resolution. We term this method, which achieves antigen

profiling and cell isolation via ferrohydrodynamic forces acting on cellular magnetic contents in a quantitative and multimodal manner, quantitative ferrohydrodynamic cell separation (qFCS). We show that qFCS allows the sorting of rare cells into multiple cell-collection chambers in a prototype qFCS device that integrates cellular "diamagnetophoresis" and "magnetophoresis" in biocompatible ferrofluids in a continuous-flow microfluidic device, leading to an overall 96.49% recovery of rare cells with a high cell purity of 98.72% across multiple cell lines. We find that qFCS has a very high level of sensitivity and is able to quantitatively profile rare cells' antigen-binding capacities accurately even when they are present at ~1:50,000 target to background cell frequency and when the cellular antigen expressions are low. The profiled cells are isolated simultaneously into multiple cell-collection chambers of the qFCS device according to the levels of their antigen bindings, resulting in a multimodal isolation method that can differentiate target cells with subtle cellular magnetic content differences. qFCS offers high-performance antigen

profiling and cell isolation that is not available in existing magnetism-based microfluidic methods (Supporting Information Table S1). 4,16-26 In the next sections, we discuss the theoretical background of qFCS, the design and calibration of qFCS for specific cell applications, the evaluation of qFCS in recovering rare cells and profiling rare cells' antigen-binding capacities, and the application of qFCS in T lymphocyte profiling and isolation via a low-expression CD154 surface antigen.

RESULTS AND DISCUSSION

Theory of Quantitative Ferrohydrodynamic Cell Separation. The goal of the qFCS method is to simultaneously provide quantitative information about the antigen-binding capacity within the rare cells and isolate rare cells based on their antigen-binding capacity in a multimodal manner. This goal is achieved through a qFCS device that can perform cell isolation according to cellular magnetic content, a dimensionless variable defined as the volume fraction of magnetic materials in a magnetically labeled cell. In this section, cellular magnetic content is shown to correlate to the cell's antigen-binding capacity. We first discuss the relationship between antigen-binding capacity and cellular magnetic content, then derive the governing equations for qFCS to guide the design and calibration of its devices.

Linking Cellular Magnetic Content of a Cell-Bead Complex to Its Surface Antigen-Binding Capacity. The predominant approaches in magnetic cell labeling include direct and indirect labels.²⁷ Direct labeling uses primary antibodies conjugated to magnetic beads, in order to selectively bind to cells that express the corresponding antigen molecules. On the other hand, indirect labeling, a two-step process, first uses a primary antibody against a specific cell surface antigen, then uses a secondary antibody conjugated to a magnetic bead to bind to the primary antibody through its secondary binding sites. Here we derive equations to relate the cellular magnetic content $\phi_{\text{cell-beads}}$ (a dimensionless variable, defined as the volume fraction of magnetic materials in a magnetically labeled cell) from its magnetic bead labeling to its surface antigen-binding capacity. We first consider the more commonly used indirect magnetic labeling process. This relationship derived for indirect labeling also holds true for the case of direct labeling (Supporting Information, Figure S1). The indirect magnetic labeling process is illustrated in Figure 1a, where a primary antibody with secondary binding sites is first bound to a specific antigen on a cell's surface. Magnetic beads with secondary antibodies then bind to the secondary binding sites on the primary antibody, which forms a magnetic cell-beads complex. The total number of magnetic beads bound to a single cell's surface through indirect labeling is 19,28,29

$$n_{\text{magnetic-beads}} = \alpha \times \beta \times \gamma \tag{1}$$

where α is the cell surface antigen-binding capacity, which is a quantitative measure representing the number of the primary antibodies bound to the cell. α depends on three parameters, including the total number of binding sites of both specific and nonspecific antigens on the cell surface, the fraction of antigens (specific and nonspecific) bound by the primary antibodies, and the valence of the primary antibody (i.e., the number of antigen-binding sites occupied by one primary antibody). β is the antibody amplification due to the secondary antibody

binding to multiple sites on the primary antibody. β is also a quantitative measure that corresponds to the number of secondary antibodies per primary antibody. It depends on three parameters, including the number of binding sites on the primary antibody recognized by the secondary antibody, the fraction of binding sites on the primary antibody that are bound by the secondary antibody, and the valence of secondary antibody binding (i.e., the number of secondary binding sites occupied by one secondary antibody). Finally, γ represents the number of magnetic beads conjugated to each secondary antibody. For a more detailed derivation and explanation of eq 1, the readers can refer to the Supporting Information and previous publications.

Equation 1 shows that the total number of magnetic beads bound to a single cell's surface through indirect magnetic labeling is determined by three parameters: α (antigen-binding capacity, the number of the primary antibodies bound to the cell), β (antibody amplification, the number of secondary antibodies per primary antibody), and γ (the number of magnetic beads conjugated to each secondary antibody). For cells used in this study, we assume that both β and γ are constant for the secondary antibody and magnetic beads when they are made from the same batch. As a result, the total number of magnetic beads $n_{\text{magnetic-beads}}$ bound to a single cell's surface becomes proportional to the remaining variable, cell surface antigen-binding capacity α , which corresponds to the number of the primary antibodies bound to each cell.

$$n_{\text{magnetic-beads}} = k\alpha$$
 (2)

where $k=\beta\times\gamma$ is assumed to be a constant for the same batch of secondary antibody modified magnetic beads. For direct magnetic labeling, antibody amplification is not present, which leads to $\beta=1$. As a result, in both direct and indirect labeling processes, $n_{\rm magnetic\text{-}beads}$ appears to have a linear relationship with α when α is relatively small. However, as α increases, the available area on a cell's surface becomes limited for magnetic bead binding, and $n_{\rm magnetic\text{-}beads}$ could saturate due to steric hindrance between neighboring magnetic beads. We show in the Supporting Information that the linear relationship in eq 2 between $n_{\rm magnetic\text{-}beads}$ and α is still valid for the cells and magnetic beads used in this study because $n_{\rm magnetic\text{-}beads}$ is below the estimated saturation number (Supporting Information Figure S2). For a detailed discussion on the steric hindrance due to magnetic beads, the readers can refer to the Supporting Information and previous publications.

We now establish the relationship between the cellular magnetic content $\phi_{\text{cell-beads}}$ and the total number of magnetic beads $\phi_{\text{magnetic-beads}}$ bound to a single cell's surface, thus the cell surface antigen-binding capacity α . The cellular magnetic content $\phi_{\text{cell-beads}}$ of a cell-beads complex is defined as

$$\phi_{\rm cell-beads} = \frac{V_{\rm magnetic-content}}{V_{\rm cell-beads}} \eqno(3)$$

where $V_{\rm magnetic-content}$ is the volume of magnetic materials of the cell—beads complex, and $V_{\rm cell-beads}$ is the total volume of the cell—beads complex including the cell and magnetic beads and has the following expression:

$$V_{\text{cell-beads}} = \frac{\pi D_{\text{cell}}^3}{6} + n_{\text{magnetic-beads}} \times \frac{\pi D_{\text{magnetic-bead}}^3}{6} \tag{4}$$

where the spherical diameter of the cell is D_{cell} and the diameter of a single magnetic bead is $D_{\text{magnetic-bead}}$. Substituting

eq 4 into eq 3, we have the following expression to relate the cellular magnetic content $\phi_{\text{cell-beads}}$ to the total number of magnetic beads $n_{\text{magnetic-beads}}$ bound to a single cell's surface:

$$\phi_{\text{cell-beads}} = \frac{n_{\text{magnetic-beads}} \times \frac{\pi D_{\text{magnetic-bead}}^3}{6} \times \phi_{\text{magnetic-bead}}}{\frac{\pi D_{\text{cell}}^3}{6} + n_{\text{magnetic-beads}} \times \frac{\pi D_{\text{magnetic-bead}}^3}{6}}{6}}$$

$$= \frac{n_{\text{magnetic-beads}} \times D_{\text{magnetic-bead}}^3 \times \phi_{\text{magnetic-bead}}}{D_{\text{cell}}^3 + n_{\text{magnetic-beads}} \times D_{\text{magnetic-bead}}^3}$$
(5)

The relationship between the cellular magnetic content $\phi_{\text{cell-beads}}$ and the number of magnetic beads $\phi_{\text{magnetic-beads}}$ on the cell surface in eq 5 can be approximated as a linear relationship when the cellular diameters are constant (Supporting Information Figure S3). However, for realistic cellular applications, cell diameters are heterogeneous; thus we need to take into account its effect. For this purpose, eqs 2 and 5 are combined and simplified assuming $D_{\text{cell}}^3 \gg n_{\text{magnetic-beads}} \times D_{\text{magnetic-bead}}^3$ (the diameter of magnetic beads $\phi_{\text{magnetic-beads}}$ in this study is ~ 10 times smaller than that of a cell D_{cell}), which leads to the following relationship between the cellular magnetic content $\phi_{\text{cell-beads}}$ and the cell's surface antigenbinding capacity α :

$$\phi_{\text{cell-beads}} = (kD_{\text{magnetic-bead}}^{3}\phi_{\text{magnetic-bead}}) \frac{\alpha}{D_{\text{cell}}^{3}}$$
(6)

Equation 6 shows that the cellular magnetic content $\phi_{\text{cell-beads}}$ is proportional to a "cell volumetric antigen-binding capacity" α/D_{cell}^3 when other parameters k, $D_{\text{magnetic-bead}}^3$ and $\phi_{\text{magnetic-beads}}$ are constant. Equation 6 can be further transformed by introducing a "cell surface density of antigen-binding capacity" $\alpha_{\text{S}} = \alpha/(\pi D_{\text{cell}}^2)$, which leads to

$$\phi_{\text{cell-beads}} = (\pi k D_{\text{magnetic-bead}}^{3} \phi_{\text{magnetic-bead}}) \frac{\alpha_{\text{S}}}{D_{\text{cell}}}$$
(7)

Equation 7 shows that the cellular magnetic content $\phi_{\text{cell-beads}}$ is proportional to the ratio of surface density of antigenbinding capacity to cellular diameter $\alpha_{\text{S}}/D_{\text{cell}}$.

Equations 6 and 7 relate an experimentally measurable entity—cellular magnetic content $\phi_{\text{cell-beads}}$ —to cells' intrinsic properties including their diameters and antigen-binding capacities. The relationships between cellular magnetic content $\phi_{\text{cell-beads}}$ and the cell's surface antigen-binding capacity α , or the cell's surface density of antigen-binding capacity α_s , depend on the cellular diameter. As a result, once the cellular magnetic content $\phi_{\text{cell-beads}}$ and cellular diameter D_{cell} are determined, we can use them to calculate the antigen-binding capacity or its density. In the next section, we introduce the governing equations of the quantitative ferrohydrodynamic cell separation, which enables us to experimentally measure the cellular magnetic content $\phi_{\text{cell-beads}}$.

Governing Equations of qFCS. Given that in this study cellular magnetic content $\phi_{\text{cell-beads}}$ is related to the cell's surface antigen-binding capacity α and the cell's surface density of antigen-binding capacity α_{S} , we aim to develop a microfluidic technology that can experimentally quantify $\phi_{\text{cell-beads}}$ among a cell population while simultaneously isolating cells based on their $\phi_{\text{cell-beads}}$. We achieved this goal by integrating cellular "diamagnetophoresis" and "magnetophoresis" in biocompatible ferrofluids in a continuous-flow microfluidic device. We term this method "quantitative

ferrohydrodynamic cell separation" because it can isolate cells based on the quantitative levels of an individual cell's antigen-binding capacity α . In comparison, traditional MACS only performs binary cell separation in which labeled cells are separated from unlabeled ones. ¹⁵

The working principle of qFCS is summarized in Figure 1b,c. Within a cell population, cells of interest are first rendered magnetic by either direct or indirect magnetic labeling. The cellular magnetic content $\phi_{ ext{cell-beads}}$ of a cell-beads complex after labeling becomes related to its antigen-binding capacity α . The cell population then continuously flows through a qFCS device, which has multiple stages of ferrofluids with spatially stable and variable magnetic concentrations over the course of experiments. Within the device, qFCS generates a magnetic force on the cell-beads complex, whose magnitude is dictated by the delicate balance between the cell-beads complex's magnetization from the labeling of magnetic beads and the cell-beads complex's surrounding magnetic medium: ferrofluids. When the cell-beads complex's magnetization $\mathbf{M}_{cell-beads}$ exceeds its surrounding ferrofluid's magnetization $\mathbf{M}_{\text{ferrofluid}}$, the net magnetic force on the cell-beads complex traps it in one of the stages of the device. On the other hand, when the cell—beads complex's magnetization $\mathbf{M}_{\text{cell-beads}}$ is equal to or less than its surrounding ferrofluid's magnetization M_{ferrofluid}, the net magnetic force on the cell-beads complex drives it to the next stage of the device. This way, as the cell population flows through the qFCS device, cells can be isolated into one of the chambers with a ferrofluid concentration that matches their cellular magnetic contents, as well as their antigen-binding capacity (Figure 1c).

The magnetic forces on the cell-bead complex in qFCS are introduced as follows. Under an external magnetic field, ferrofluids have a magnetization of $M_{\text{ferrofluid}}$ while the cellbeads complex possesses a magnetization of $\mathbf{M}_{cell-beads}$, due to its labeling of magnetic beads. The interaction of the cell-bead complex with the external magnetic field depends on the balance of both "magnetophoresis" and "diamagnetophoresis". Figure 1b shows that magnetophoretic force results from the conjugated magnetic beads on the cell and directs the cell toward the maximum of a nonuniform magnetic field, while diamagnetophoretic force results from the ferrofluids' magnetic nanoparticle-induced pressure imbalance on the cell's surface and directs the cell toward the minima of the magnetic field. The overall magnetic force on the cell-bead complex in the ferrofluid under an external magnetic field can be found in previous reports^{30–35} and is also derived in detail in the Supporting Information. Here we have the overall magnetic force acting on the cell-beads complex, which is the sum of the two competing forces: diamagnetophoretic and magnetophoretic forces:

$$\vec{\mathbf{F}}_{m} = \vec{\mathbf{F}}_{diamagnetophoretic} + \vec{\mathbf{F}}_{magnetophoretic}$$

$$= -\mu_{0} V_{cell-beads} \{ (\vec{\mathbf{M}}_{ferrofluid} - \vec{\mathbf{M}}_{cell-beads}) \cdot \nabla \} \vec{\mathbf{H}}$$
(8)

Equation 8 is derived in detail in the Supporting Information. We note that this magnetic force expression does not consider magnetic bead-to-bead interaction and its effect on the force experienced by the cell—beads complex. We estimated the bead-to-bead interaction and its effect on the magnetic force in the Supporting Information and found it to be negligible in our experimental conditions. From eq 8, we know that the direction and magnitude of the overall magnetic force $\vec{F}_{\rm m}$ acting on a cell—beads complex in qFCS depends delicately on

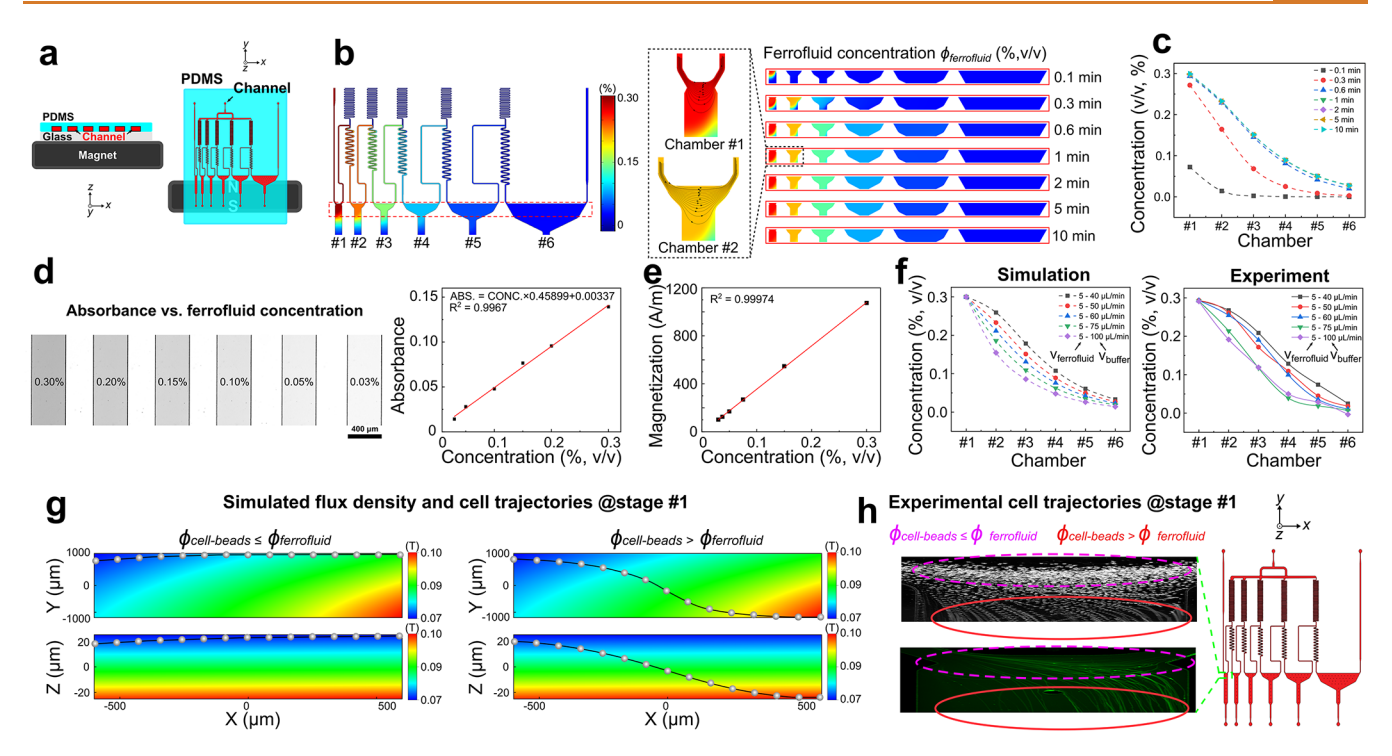


Figure 2. Design of the quantitative ferrohydrodynamic cell separation (qFCS) method for cell isolation. (a) Schematic of the qFCS device shows the location of the permanent magnet and the microfluidic channels. This configuration leads to a magnetic flux density and gradient sufficient for cell isolation. The permanent magnet (50.8 mm \times 6.35 mm \times 6.35 mm, $L \times W \times H$, N52 neodymium magnet) is placed relative to the microfluidic device, as shown here. Under such configuration, a magnetic flux density of up to 0.36 T in the x-y plane (z=0, top panel) and up to 0.28 T in the x-z plane (y=0, bottom panel) is generated (Supporting Information Figure S7). (b) (Simulation) Simulated ferrofluid concentrations ($\phi_{\text{ferrofluid}}$) in the six cell-collection chambers at different time points. In this simulation, a 0.3% (v/v) ferrofluid is injected into inlet A at a flow rate of 5 μ L min⁻¹, and a PBS buffer solution is injected into inlet B at a flow rate of 50 μ L min⁻¹. $\phi_{\text{ferrofluid}}$ in each cell-collection chamber (#1-6, red dashed rectangles) is shown at 0.1, 0.3, 0.6, 1, 2, 5, and 10 min. Spatially stable ferrofluid concentration can be established in the effective cell flow region of cell-collection chambers in 1 min. Color bar shows the magnitude of the ferrofluid concentrations. (c) (Simulation) Spatially stable and monotonically decreasing $\phi_{\text{ferrofluid}}$ profile can be established in the qFCS device after 1 min. Concentration is calculated by averaging the effective flow region in each chamber. (d) (Experiment) Bright-field images of the ferrofluid in the cell-collection chambers of the qFCS device at variable concentrations from 0.03% to 0.3% are used to determine a linear relationship between the light absorbance of ferrofluids and $\phi_{\text{ferrofluid}}$. The theory of this linear relationship is discussed in the Supporting Information. The light absorbance of the ferrofluid is calculated by $\log_{10}(i_0/i_{\text{ferrofluid}})$, where i_0 is the mean of the grayscale value of a bright-field image without ferrofluids, and $i_{\text{ferrofluid}}$ is the mean of the grayscale value of a bright-field image with ferrofluids. The brightfield images are taken near the ferrofluid inlet (inlet A) of the qFCS device. (e) (Experiment) The linear relationship between the experimentally measured magnetization of the ferrofluid and $\phi_{\text{ferrofluid}}$. Linear fitting of the relationship ($R^2 = 0.9997$, n = 3) shows that ferrofluid magnetization is proportional to $\phi_{\text{ferrofluid}}$ as expected. (f) Simulation (left panel) and experimental (right panel) results of $\phi_{\text{ferrofluid}}$ in the cell-collection chamber at variable flow ratios (ferrofluid: buffer). The ferrofluid flow rate (inlet A, 0.3%, v/v ferrofluid) is $5 \mu L$ min while the buffer flow rate (inlet B, PBS buffer) is 40-100 µL min⁻¹. (g) (Simulation) Simulated cell trajectories in stage #1 of the qFCS device. (Left panel) In the case of $\phi_{\text{cell-beads}} \leq \phi_{\text{ferrofluid}}$, in which the cellular magnetic content $\phi_{\text{cell-beads}}$ of a cell-beads complex (10 μ m diameter, labeled with five magnetic beads (magnetic beads: 1.05 μ m diameter, 11.5% (v/v) magnetic content)) is less than or equal to the ferrofluid concentration $\phi_{\text{ferrofluid}}$ in that stage (stage #1), the cell-beads complex is driven to the next stage of the device. (Right panel) In the case of $\phi_{\text{cell-beads}} > \phi_{\text{ferrofluid}}$, in which the cellular magnetic content $\phi_{\text{cell-beads}}$ of a cell-beads complex (10 μ m diameter, labeled with 30 magnetic beads (magnetic beads: 1.05 μ m diameter, 11.5% (v/v) magnetic content)) is larger than the ferrofluid concentration $\phi_{\text{ferrofluid}}$ in that stage (stage #1), the cell-beads complex is trapped at stage #1. The ferrofluid (0.3% v/v) flow rate is 5 µL min⁻¹ and buffer flow rate is 50 μL min⁻¹ in the simulation. Color bar shows the magnitude of the magnetic flux density. (h) (Experiment) Phase contrast (top) and fluorescent (bottom) images of cell trajectories of human white blood cells (WBCs) labeled with magnetic beads targeting CD45 in the qFCS device (stage #1). Ferrofluid concentration is 0.3% (v/v), ferrofluid flow rate is 5 μ L min⁻¹, and buffer flow rate is 50 μ L min⁻¹. Purple dashed ellipse shows the cell-beads complexes with $\phi_{\text{cell-beads}} \leq \phi_{\text{ferrofluid}}$, while the red solid ellipse shows the cell-beads complexes with $\phi_{\text{cell-beads}} > \phi_{\text{ferrofluid}}$. The green box on the device schematic shows the location of the observation window (stage #1).

the product of the cell-beads complex's volume and the magnetization contrast between the cell-beads complex and the ferrofluid, i.e., the term $V_{\text{cell-beads}}(\vec{\mathbf{M}}_{\text{ferrofluid}}-\vec{\mathbf{M}}_{\text{cell-beads}})$ in eq. 8. We note that similar to the case where a cell-beads complex's magnetization $\vec{\mathbf{M}}_{\text{cell-beads}}$ is the product of its magnetic content $\phi_{\text{cell-beads}}$ and the bulk magnetization of magnetic materials in the magnetic bead $\vec{\mathbf{M}}_{\text{bulk_cell-beads}}$, a ferrofluid's magnetization $\vec{\mathbf{M}}_{\text{ferrofluid}}$ is also the product of its magnetic content $\phi_{\text{ferrofluid}}$ (often referred to as ferrofluid

concentration, which is the volume fraction of magnetic materials in the ferrofluid) and the bulk magnetization of magnetic materials in the ferrofluid $\vec{M}_{\text{bulk ferrofluid}}$:

$$\vec{\mathbf{M}}_{\text{ferrofluid}} = \phi_{\text{ferrofluid}} \times \vec{\mathbf{M}}_{\text{bulk-ferrofluid}}$$
 (9)

Now we consider the case in which a cell—beads complex flows through one of the stages of the ferrofluids in the qFCS (Figure 1c). When the condition of $\vec{M}_{\text{cell-beads}} \leq \vec{M}_{\text{ferrofluid}}$ is

met, i.e., $\phi_{\rm cell-beads} \leq \phi_{\rm ferrofluid}$ assuming the ferrofluid and the magnetic beads are made of the same magnetic material, the diamagnetophoretic force overcomes the magnetophoretic force and drives the cell-beads complex to the next stage against a hydrodynamic viscous drag. On the other hand, when the condition of $M_{cell-beads} > M_{ferrofluid}$ is met, i.e., $\phi_{cell-beads} >$ $\phi_{ ext{ferrofluid}}$, the magnetophoretic force outweighs the diamagnetophoretic force and traps the cell-beads complex in that stage. This way, each stage of the qFCS with a variable ferrofluid concentration $\phi_{ ext{ferrofluid}}$ can trap cell-beads complexes with matching cellular magnetic content. Because cellular magnetic content $\phi_{\text{cell-beads}}$ is shown to correlate to the cell's surface antigen-binding capacity α and the cell's surface density of antigen-binding capacity $\alpha_{\rm S}$, we can then use qFCS to isolate cells based on their binding levels of a specific antigen, while also measuring the distribution of that antigen's binding capacity among the cell population.

We applied the above-mentioned qFCS principle to the design and fabrication of a prototype device, which consists of a microfluidic device and a permanent magnet (Figure 1c). The microfluidic device, shown in Figure 1d,e, has six stages of spatially stable and concentration variable ferrofluids that can be generated and maintained over the course of the experiments (Figure 1f, top panel). Each stage of qFCS has a corresponding cell-collection chamber (dashed boxes in Figure 1e) that is used to collect cell-beads complexes with a matching cellular magnetic content to the ferrofluid concentration in that stage. This prototype device could isolate human white blood cells (WBCs) into the cell-collection chambers based on their cellular magnetic contents $\phi_{\text{cell-beads}}$ and their antigen-binding capacity of CD45 (Figure 1f, bottom panel). In the following section, we discuss the design considerations and calibration processes of the prototype qFCS device for specific cell separations.

Design and Calibration of qFCS. Design of qFCS. From the discussions in the previous section, we learn that the following outcomes are desired in order to apply the qFCS method for cell separations: (1) generation and maintenance of multiple spatially stable ferrofluid stages with variable concentrations; (2) trapping of the cell-beads complex in a stage that satisfies the condition of $\phi_{ ext{cell-beads}} > \phi_{ ext{ferrofluid}}$. We addressed these considerations through a prototype qFCS device illustrated in Figures 1d,e and 2a. In this device design, a ferrofluid flow with cells (inlet A, Figure 1e) is continuously mixed with a buffer flow (inlet B, Figure 1e) and diluted in its concentration as it flows through the six stages (#1-6, Figure 1e) of the device. In this process, six cell-collection chambers (dashed box #1-6, Figure 1e) with spatially stable and decreasing ferrofluid concentrations are generated and sustained over time to allow for cell isolations in these chambers. A permanent magnet (Figure 2a) is positioned underneath the microfluidic device and close to the chambers, so that sufficient magnetic forces (Supporting Information Figure S7) can be produced to either trap the cell-bead complex in one of the cell-collection chambers or drive it to the next stage of the device, based on the contrast between the cellular magnetic content and the ferrofluid concentration in that stage. Separated cells in each cell-collection chamber can be characterized for their cellular magnetic contents or collected via the outlets (outlets, Figure 1e) for further analysis. In designing this prototype device, we chose the number of stages and cell-collection chambers to be six in order to balance the complexity of the device and the ability to

separate cells in a multimodal manner. The rationale to balance device complexity and multimodal cell separation can be explained as follows: as the number of stages and cellcollection chambers in a qFCS device increase, the complexity of the overall microfluidic channels, especially the number of microchannels used for ferrofluid dilution (serpentine-shaped channels in Figure 2b) increases, which leads to a reduced maximum cell flow rate and cell-processing throughput of the device; on the other hand, as the stages and cell-collection chambers decrease, the modes (cell-collection chambers) of the magnetic content-based cell isolation decrease. The current qFCS device has six stages and cell-collection chambers so that it can process a reasonable amount of cell samples at a \sim 5 μ L min^{-1} flow rate and a ~ 30,000 cell min^{-1} throughput, while still providing six modes (cell-collection chambers) that can completely separate cells with a minimum difference in their cellular magnetic contents.

We proceeded to calibrate the qFCS device to evaluate its ability to isolate and profile cells based on cellular magnetic content. The device was first examined for its ability to generate and maintain six stages of spatially stable and concentration-variable ferrofluids over time. Simulated profiles in Figure 2b,c show that spatially stable ferrofluid concentrations in the effective cell flow region of the cell-collection chambers can be established in ~1 min and maintained with a continuous flow of ferrofluids (inlet A, Figure 1e) and buffer (inlet B, Figure 1e). The effective cell flow region of cellcollection chambers is defined as the region where the cells can travel to. In order to experimentally measure the ferrofluid concentrations in the qFCS cell-collection chambers, we first established a linear relationship between a ferrofluid's light absorbance and its concentration (volume fraction of magnetic materials) in Figure 2d. The theory of this linear relationship is derived in the Supporting Information and Figure S5. Using this linear relationship, together with the fact that a ferrofluid's magnetization is proportional to its concentration (Figure 2e), we obtained the ferrofluid concentration in the qFCS cellcollection chambers based on its light absorbance through imaging. This enabled us to investigate the ferrofluid concentration profiles in these chambers at variable flow rates and flow ratios (ferrofluid: buffer). Figure 2f shows the relationship between the ferrofluid concentrations in the cellcollection chambers at a constant ferrofluid flow rate, but with variable flow ratios (ferrofluid: buffer). Both simulation and experimental data in Figure 2f confirm that monotonically decreasing ferrofluid concentrations can be established in the qFCS device across stages and cell-collection chambers #1-6. Lowering flow ratios between the ferrofluid and the buffer accelerates the dilution of ferrofluids (Figure 2f) while keeping the flow ratio between the ferrofluid and buffer constant results in the same decreasing trend of dilution (Supporting Information Figure S6). From these results, we confirm that (1) a total of six spatially stable ferrofluid concentrations can be established in ~1 min in the qFCS device and sustained over time to allow for subsequent cell profiling and isolation; (2) the maximum of the ferrofluid concentrations in the qFCS device is determined by the concentration of the starting ferrofluid flow (Supporting Information Figure S8), while the decreasing trend of the ferrofluid concentrations across six stages and cell-collection chambers in the qFCS device is determined by the flow ratio between the ferrofluid and the buffer. These findings allow us to design patterns of ferrofluid

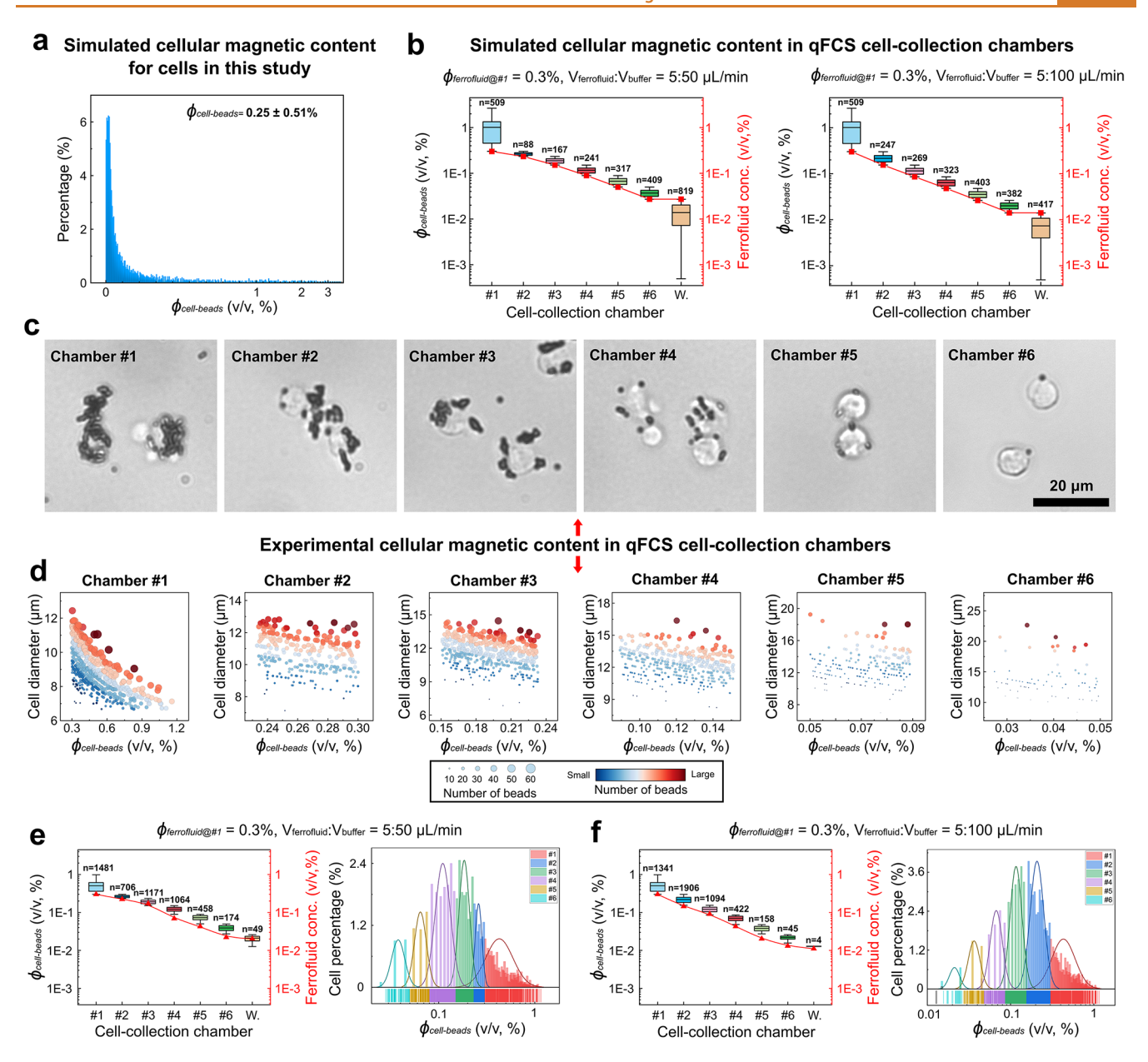


Figure 3. Calibration of the quantitative ferrohydrodynamic cell separation (qFCS) method for cell isolation. (a) (Simulation) Estimated distribution of cellular magnetic contents ($\phi_{\text{cell-beads}}$) for the cells used in this study. $\phi_{\text{cell-beads}}$ is $0.25 \pm 0.51\%$ (v/v, mean \pm s.d., n = 2,550), for the cellular diameter and magnetic beads used in this study (cell diameter: $5-30 \mu m$, number of magnetic beads per cell: 1-50, each magnetic bead has a diameter of 1.05 μ m and a magnetic content of 11.5% (v/v)). (b) (Simulation) (Left panel) Distribution of $\phi_{cell-beads}$ in the six cell-collection chambers of the qFCS device under the following conditions: a ferrofluid flow rate of 5 μ L min⁻¹ and a buffer flow rate of 50 μ L min⁻¹. $\phi_{\text{cell-beads}}$ (%, v/v, mean \pm s.d.) are 1.01 \pm 0.74 (chamber #1, n = 509), 0.26 \pm 0.02 (chamber #2, n = 88), 0.19 \pm 0.02 (chamber #3, n = 167), 0.12 ± 0.02 (chamber #4, n = 241), 0.07 ± 0.01 (chamber #5, n = 317), 0.04 ± 0.01 (chamber #6, n = 409), and 0.01 \pm 0.01 (waste outlet, labeled as "W", n = 819). (Right panel) Distribution of $\phi_{\text{cell-beads}}$ in the six cell-collection chambers of the qFCS device under the following conditions: a ferrofluid flow rate of 5 μ L min⁻¹ and a buffer flow rate of 100 μ L min⁻¹. $\phi_{cell-beads}$ (%, v/v, mean \pm s.d.) are 1.01 ± 0.74 (chamber #1, n = 509), 0.22 ± 0.04 (chamber #2, n = 247), 0.12 ± 0.02 (chamber #3, n = 269), 0.06 ± 0.01 (chamber #4, n = 269) = 323), 0.03 ± 0.01 (chamber #5, n = 403), 0.02 ± 0.004 (chamber #6, n = 382), and 0.01 ± 0.004 (waste outlet, labeled as "W", n = 417). The starting ferrofluid concentration ($\phi_{\text{ferrofluid} \# 1}$) is 0.3% (v/v) in both simulations. (c) (Experiment) Bright field images of anti-CD45modified magnetic beads labeled white blood cells (WBCs) isolated in the cell-collection chambers of the qFCS device. Isolated WBCs in each cell-collection chamber are imaged to extract cell diameters and count the number of magnetic beads per cell to calculate $\phi_{\text{cell-beads}}$. (d) (Experiment) Distribution of cell diameters and $\phi_{ ext{cell-beads}}$ in each cell-collection chamber. The number of magnetic beads on each cell is shown. (e) (Experiment) Distribution of $\phi_{\text{cell-beads}}$ cell-beads complexes in each cell-collection chamber of the qFCS device is summarized for WBC isolation based on their CD45 binding capacity. (Left panel) $\phi_{\text{cell-beads}}$ (%, v/v, mean \pm s.d.) of WBCs are measured to be 0.51 \pm 0.18 (chamber #1, n = 1,481), 0.26 \pm 0.02 (chamber #2, n = 706), 0.19 \pm 0.02 (chamber #3, n = 1,171), 0.12 \pm 0.02 (chamber #4, n = 1,171) 1,064), 0.07 ± 0.01 (chamber #5, n = 458), 0.04 ± 0.01 (chamber #6, n = 174), and 0.02 ± 0.00 (waste outlet, labeled as "W", n = 49). (Right panel) The percentages of cells in each cell-collection chamber in the qFCS device after cell isolation. This experiment is conducted with a starting ~5,000 WBCs at a concentration of 25,000 cells/mL that are indirectly labeled with anti-CD45 magnetic beads (magnetic beads: 1.05 µm diameter, 11.5% (v/v) magnetic volume fraction) and processed in the qFCS device with the following conditions: starting

Figure 3. continued

ferrofluid concentration $\phi_{\text{ferrofluid}@\#1}$ 0.3% (v/v), ferrofluid flow rate 5 μ L min⁻¹, buffer flow rate 50 μ L min⁻¹. (f) (Experiment) Similar study of WBC isolation based on their CD45 binding capacity in the qFCS device as in (d), except that the buffer flow rate is 100 μ L min⁻¹. (Left panel) $\phi_{\text{cell-beads}}$ (%, v/v, mean \pm s.d.) are 0.52 \pm 0.15 (chamber #1, n = 1,341), 0.22 \pm 0.04 (chamber #2, n = 1,906), 0.12 \pm 0.02 (chamber #3, n = 1,094), 0.07 \pm 0.01 (chamber #4, n = 422), 0.04 \pm 0.01 (chamber #5, n = 158), 0.02 \pm 0.00 (chamber #6, n = 45), and 0.01 \pm 0.00 (waste outlet, labeled as "W", n = 4). (Right panel) The percentages of cells in each cell-collection chamber in the qFCS device after cell isolation.

Table 1. Quantification of Multimodal and Nonoverlapping Cell Profiling and Isolation Based on Cellular Magnetic Contents in the qFCS Device

				range of cellular magnetic contents in the cell-collection chambers (v/v, %)					
starting ferrofluid concentration (v/v, %)	flow ratio (ferrofluid: buffer)	sources of	range of cellular magnetic contents that can be profiled (v/v, %)	cell collection chambers #1	cell collection chambers #2	cell collection chambers #3	cell collection chambers #4	cell collection chambers #5	cell collection chambers #6
0.3	$V_{\text{ferrofluid}}:V_{\text{buffer}} = 5.50 \mu \text{L min}^{-1}$	Simulation	0.00049-3.64	0.30-3.64	0.23-0.30	0.15-0.23	0.09-0.15	0.05-0.09	0.03-0.05
		Experiment	0.013-1.16	0.30 - 1.16	0.23-0.30	0.15 - 0.23	0.09 - 0.15	0.05-0.09	0.03-0.05
	$V_{\text{ferrofluid}}:V_{\text{buffer}} = 5:100\mu\text{L min}^{-1}$	Simulation	0.00049 - 3.64	0.30 - 3.64	0.15-0.30	0.09 - 0.15	0.05-0.09	0.03-0.05	0.01 - 0.03
		Experiment	0.012-1.18	0.30 - 1.17	0.15-0.30	0.09 - 0.15	0.05-0.09	0.03-0.05	0.02 - 0.03
0.03	$V_{\text{ferrofluid}}: V_{\text{buffer}} = 5:50 \ \mu\text{L min}^{-1}$	Simulation	0.00049-3.64	0.030- 3.640	0.023- 0.030	0.015- 0.023	0.009- 0.015	0.005- 0.009	0.003-0.005
	$V_{\text{ferrofluid}}:V_{\text{buffer}} = 5:100\mu\text{L min}^{-1}$	Simulation	0.00049-3.64	0.030- 3.640	0.015- 0.030	0.009- 0.015	0.005- 0.009	0.003- 0.005	0.001-0.003

concentration in the qFCS device according to specific cell separation needs.

The qFCS device was also examined through simulation and experiments for its ability to trap cell-beads complexes in a cell-collection chamber that satisfies the condition of $\phi_{ ext{cell-beads}}$ > $\phi_{\rm ferrofluid}$. We chose a total flow rate for the qFCS device that was sufficiently slow so that cells passing through the device were predominately distinguished based on the contrast of their cellular magnetic contents and the ferrofluid concentration (Supporting Information Figure S9). Simulated cell trajectories in Figure 2g show that the stages and cell-collection chambers in the qFCS device can successfully differentiate cell-beads complexes based on the contrast of their magnetic content $\phi_{
m cell-beads}$ and the concentration of surrounding ferrofluids $\phi_{\text{ferrofluid}}$. For example, in the case of $\phi_{\text{cell-beads}} \leq$ $\phi_{\text{ferrofluid}}$ shown in the left panel of Figure 2g, diamagnetophoretic force on the cell-beads complex equals or outweighs the magnetophoretic force and drives it to the next stage of the device. In the case of $\phi_{
m cell-beads} > \phi_{
m ferrofluid}$ in the right panel of Figure 2g, magnetophoretic force exceeds diamagnetophoretic force on the cell-beads complex and traps it in the current stage. Experimental images of the cell trajectories in Figure 2h reveal that the magnetic force generated by the permanent magnet (Supporting Information Figure S7) in the qFCS device resulted in a clear differentiation of two groups of cells based on their magnetic contents ($\phi_{ ext{cell-beads}} \leq \phi_{ ext{ferrofluid}}$ or $\phi_{\rm cell-beads} > \phi_{\rm ferrofluid})$ in one of the stages (stage #1). In summary, through both simulation and experiments, we designed a qFCS device that can generate and sustain spatially stable and variable ferrofluid concentrations across its six stages and cell-collection chambers to enable multimodal magnetic content-based cell profiling and isolation. This device is calibrated in the next section to optimize its operating parameters for specific cell applications.

Calibration of qFCS. We now have a qFCS device that can generate and sustain six stages of decreasing ferrofluid concentrations $\phi_{\text{ferrofluid}}$ and profile and isolate cells based on cellular magnetic contents. However, for specific cell types, the operating parameters of this device, including its starting

ferrofluid concentration and flow ratios between the ferrofluid and the buffer, should be carefully optimized by taking into account the physical and magnetic properties of the cells. The cells used in this study, including cancer cells and peripheral blood mononuclear cells (PBMCs), are estimated to have a physical diameter of 5–30 μ m, with each cell being indirectly labeled with 1-50 magnetic beads. The magnetic beads used in this study have a 1.05 μ m diameter and an 11.5% volume fraction of magnetic materials. Using these physical and magnetic properties, we estimated the distribution of cellular magnetic contents among the cell population to be 0.25 \pm 0.51% (v/v, mean \pm s.d., n = 2,550) in Figure 3a. The estimated cellular magnetic content instructed us to choose the starting ferrofluid concentration to be ${\sim}0.3\%$ (v/v) so that the majority of the cell-beads complexes can be isolated and profiled in the six cell-collection chambers of the qFCS device.

Prior to the cell experiments, we used simulations to investigate the range of cellular magnetic contents in the qFCS's cell-collection chambers. Figure 3b shows the data in which a total of 2,550 cell-beads complexes, with their physical and magnetic properties sampled from Figure 3a, were simulated using different flow ratios (ferrofluids: buffer). First, we learn that spatially stable and variable concentrations of ferrofluids were generated and sustained in both simulations. In both cases, the maximum ferrofluid concentration was decided by the starting ferrofluid concentration $\phi_{ ext{ferrofluid}@\#1}$, which was 0.3% (v/v). The decreasing trend of ferrofluid concentrations across six stages was decided by the flow ratio between the ferrofluid and the buffer. Having a larger flow ratio between the ferrofluid and buffer led to a faster dilution of ferrofluids, therefore a smaller minimum ferrofluid concentration $\phi_{\text{ferrofluid}@\#6}$ at the last stage (sixth stage) of the device. Second, cell-beads complexes were successfully isolated into one of the cell-collection chambers with matching cellular magnetic content and ferrofluid concentration. For example, the n^{th} cell-collection chamber with a ferrofluid concentration of $\phi_{ ext{ferrofluid} \# n}$ can isolate cell—beads complexes with a cellular magnetic content $\phi_{\text{cell-beads}}$ that falls into the range of $\phi_{\text{ferrofluid}@\#n-1} \geq \phi_{\text{cell-beads}} > \phi_{\text{ferrofluid}@\#n}$. We summarize the

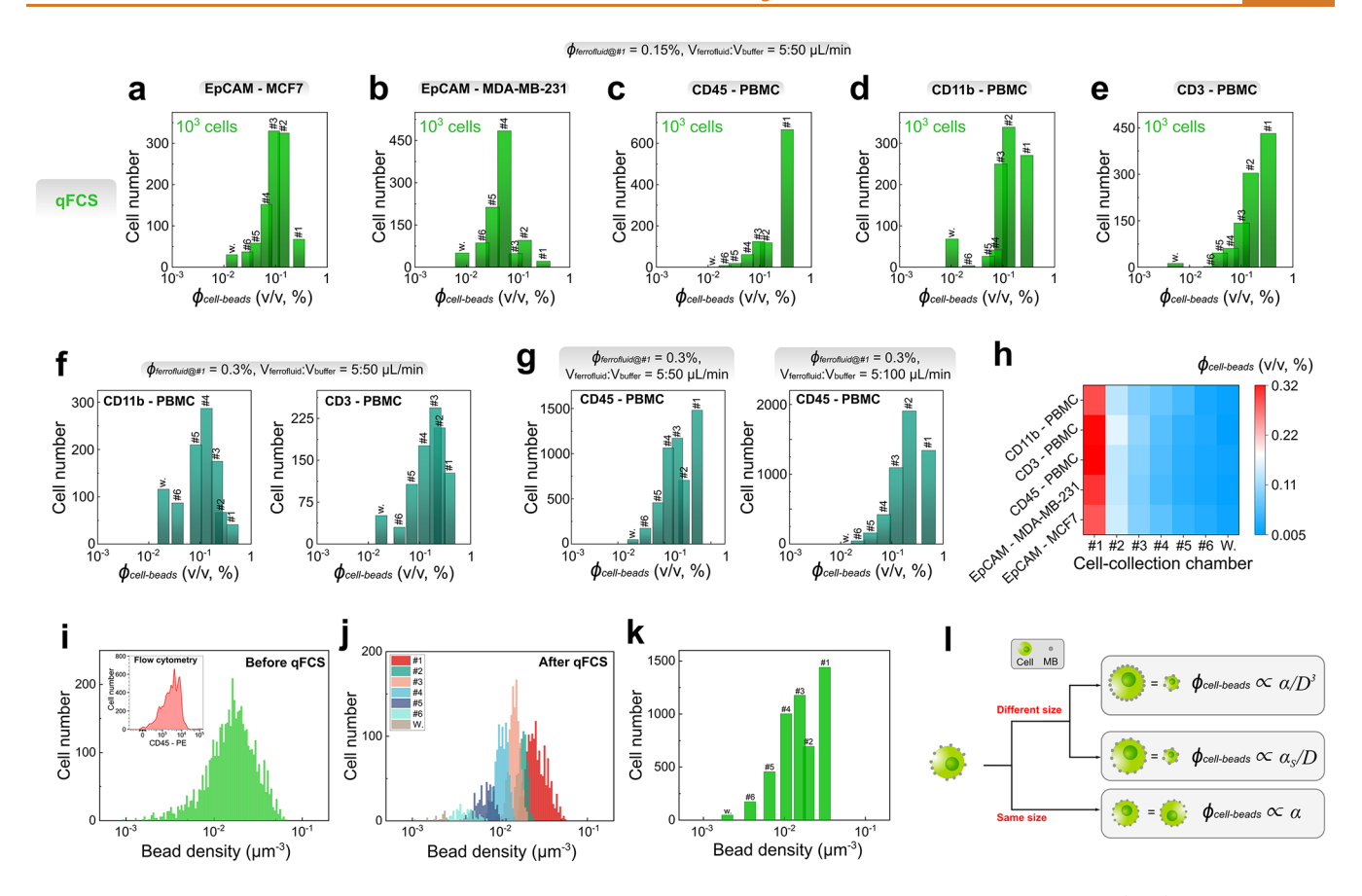


Figure 4. Experimental validation of the qFCS device for its capabilities of quantifying antigen-binding capacity. (a-e) qFCS quantifies "volumetric antigen-binding capacity" in cultured cancer cells and peripheral blood mononuclear cells (PBMCs) through cellular magnetic contents $\phi_{\text{cell-beads}}$. Five separate experiments were conducted using qFCS. Each qFCS experiment started with \sim 1,000 cells (MCF7 breast cancer, MDA-MB-231 breast cancer, or PMBCs), which were labeled with magnetic beads (diameter: 1.05 μm; magnetic content: 11.5% (v/ v)) through indirect labeling of respective antibodies (anti-EpCAM for MCF7 breast cancer cells or MDA-MB-231 breast cancer cells, anti-CD45, anti-CD3, and anti-CD11b for PMBCs). These ~1,000 labeled cells were spiked into ~1,000,000 unlabeled PBMCs with a final volume of 200 μ L and then processed by the qFCS devices. qFCS device processing parameters included a starting ferrofluid concentration $\phi_{\text{ferrofluid}}$ of 0.15% (v/v), a ferrofluid flow rate of 5 μ L min⁻¹, and a buffer flow rate of 50 μ L min⁻¹. Isolated cells in the chambers of the qFCS device were counted and calculated for their cellular magnetic contents $\phi_{\text{cell-beads}}$. The numbers in the qFCS plots are the number of cellcollection chambers. (a) Cellular magnetic content $\phi_{\text{cell-beads}}$ targeting EpCAM for MCF7 breast cancer cells. (b) $\phi_{\text{cell-beads}}$ targeting EpCAM for MDA-MB-231 breast cancer cells. (c) $\phi_{\text{cell-beads}}$ targeting CD45 for PMBCs. (d) $\phi_{\text{cell-beads}}$ targeting CD11b for PMBCs. (e) $\phi_{\text{cell-beads}}$ targeting CD3 for PMBCs. (f) $\phi_{cell-beads}$ targeting CD11b and CD3 for PMBCs with a 0.3% (v/v) starting ferrofluid concentration. (g) Comparison of $\phi_{\text{cell-beads}}$ targeting CD45 for PMBCs with different flow ratios. (h) Means of $\phi_{\text{cell-beads}}$ in each cell-collection chamber of the qFCS device. The means are calculated using experimental data from (a)–(e). $\phi_{\text{cell-beads}}$ (%, v/v) are 0.28–0.34 (chamber #1), 0.13–0.15 (chamber #2), 0.09-0.10 (chamber #3), 0.05-0.07 (chamber #4), 0.03-0.05 (chamber #5), 0.02-0.03 (chamber #6), and 0.005-0.01 (waste outlet). (i) Comparison between flow cytometry and qFCS in profiling CD45 density in PBMCs. qFCS used magnetic bead density, which was proportional to antigen-binding capacity density. (j) qFCS profiled and isolated cells based on CD45 density into its six cellcollection chambers. (k) Mean magnetic bead densities in each cell-collection chamber. (l) Three modes of antigen-binding capacity based operation of qFCS, depending on cellular diameters.

ranges of cellular magnetic contents in each cell-collection chamber when the sample passed through the device in Table 1, which shows that each chamber isolated a specific and nonoverlapping range of cellular magnetic contents. We note that the ranges of cellular magnetic contents between neighboring chambers are not uniform, mainly because of the nonlinearity in the decreasing trend of the ferrofluid concentrations in the current device. We also note that cell-collection chamber #1 has a much wider range of cellular magnetic content comparing to other chambers, because it captures any cell—bead complex that satisfies the condition $\phi_{\text{cell}-\text{beads}} > \phi_{\text{ferrofluid}@\#1}$. Third, the flow ratio between the ferrofluid and the buffer determined the decreasing trend of ferrofluid concentrations across six stages. With a larger flow

ratio (Figure 3b, left panel, $V_{\rm ferrofluid}$: $V_{\rm buffer} = 5:50~\mu L~{\rm min}^{-1}$), the decreasing trend of ferrofluid concentrations is slower, which leads to a narrower range of cellular magnetic contents that can be isolated and profiled. On the other hand, a smaller flow ratio (Figure 3b, right panel, $V_{\rm ferrofluid}$: $V_{\rm buffer} = 5:100~\mu L~{\rm min}^{-1}$) results in a faster-decreasing trend of ferrofluid concentrations, which implies a broader range of cellular magnetic contents that can be isolated and profiled (Table 1).

These simulation findings were compared with cell experiments in which \sim 5,000 WBCs with 6–23 μ m diameters, indirectly labeled with anti-CD45-modified magnetic beads, were profiled and isolated by the qFCS devices in Figure 3c–f. First, experimental images in Figure 3c,d from the WBC profiling and isolation experiments show that neighboring cell-

collection chambers in the qFCS device can differentiate cellbeads complexes based on their cellular magnetic contents $\phi_{
m cell-beads}$. In each cell-collection chamber, qFCS captures a cell subpopulation that has variable cellular diameters and a variable number of magnetic beads. Mean diameters of cells increase from chamber #1 to #6 (Supporting Information Figure S11). Within each chamber, the number of magnetic beads on cells increases as the cell diameter increases (Supporting Information Figure S12). However, the cells in each chamber have a predetermined range of cellular magnetic contents $\phi_{
m cell-beads}$ that is decided by the ferrofluid concentration in that stage, demonstrating qFCS's ability to differentiate cells based solely on $\phi_{\text{cell-beads}}$. The experimental range of cellular magnetic contents in each chamber matched the simulation data in Table 1. Second, we note that the ferrofluid concentration profiles and the range of cellular magnetic contents that can be processed from these experiments in Figure 3e,f are consistent with the simulation estimates. The comparisons of simulation and experimental data are presented in Table 1. Third, we note that the waste outlets in WBC experiments in Figure 3e,f contain a 1 to 2 orders of magnitude smaller number of cells compared to their simulation estimates in Figure 3b. This can be attributed to the fact that the simulations in Figure 3b overestimated the number of cells that have small cellular magnetic contents (large diameters with very few magnetic beads attached). Taken together, these findings validated the simulation data so that the simulation process can be used in the future to determine the operating parameters of the qFCS device, including the starting ferrofluid concentration and flow ratios between the ferrofluid and the buffer, for specific cell separation applications.

Evaluating qFCS for Simultaneous Cell Profiling and **Isolation.** *Cell Profiling by qFCS.* Using the prototype qFCS device and its optimized operating parameters, we validated the device with spiked cancer cells and PBMCs. These experiments were conducted to evaluate the performance of qFCS in both profiling antigen bindings and isolating rare cells based on their antigen bindings among a cell population. First, we evaluated the ability of qFCS in quantifying antigen-binding capacity in cultured cancer cells and PBMCs. qFCS profiles and separates cells based on the cellular magnetic content $\phi_{
m cell-beads}$, which correlates to cells' antigen-binding capacities and their cellular diameter as discussed in eqs 6 and 7. From the discussion we know that cellular magnetic content $\phi_{
m cell-beads}$ is proportional to a "cell volumetric antigen-binding capacity" α/D_{cell}^3 as well as to the ratio of antigen-binding capacity density to cellular diameter $\alpha_{\rm S}/D_{\rm cell}$. It also follows that $\phi_{\text{cell-beads}}$ is proportional to α when cellular diameters are constant. As a result, the experimental determinations of $\phi_{
m cell-beads}$ and/or $D_{
m cell}$ can be used to profile the cells' antigenbinding capacity.

The experiments in this section optimized the operating parameters of the qFCS device, including a starting ferrofluid concentration $\phi_{\text{ferrofluid}}$ of 0.15% (v/v), a ferrofluid flow rate of 5 μ L min⁻¹, and a buffer flow rate of 50 μ L min⁻¹. The parameters were chosen after evaluating the cells' physical features and magnetic labeling. Five separate cell experiments were conducted to evaluate the profiling performance of the qFCS. The qFCS device can profile cells even with a low number of target cells. Each qFCS cell experiment started with ~1,000 cells from a single culture (MCF7 breast cancer, MDA-MB-231 breast cancer, or PMBCs). The cells were indirectly

labeled with magnetic beads (diameter: 1.05 μ m; magnetic content: 11.5% (v/v)) that use antibodies targeting specific antigens on the cell surface (anti-EpCAM for MCF7 breast cancer cells or MDA-MB-231 breast cancer cells, anti-CD45, anti-CD11b, and anti-CD3 for PMBCs). Labeled cells were then spiked into ~1,000,000 unlabeled PBMCs with a final volume of 200 μ L and processed by a qFCS device. Cells in each cell-collection chamber of the device were imaged and analyzed for their cellular magnetic contents $\phi_{
m cell-beads}$ (Figure 4a−e). We note that the qFCS devices profiled the "volumetric antigen-binding capacities $\alpha/D_{\mathrm{cell}}^3$ of all five types of cells, through their cellular magnetic contents $\phi_{ ext{cell-beads}}$ at a low target to background cell frequency of 1:1,000. qFCS profiling depended sensitively on the experimental conditions including the starting ferrofluid concentration $\phi_{\text{ferrofluid}@\#1}$ and the flow ratio (ferrofluid: buffer). Figure 4f compares the difference of CD11b and CD3 profiling of PBMC between a starting ferrofluid concentration $\phi_{ ext{ferrofluid}@\#1}$ 0.3% (v/v) and 0.15% (v/ v) presented in Figure 4d,e. Shifting the starting ferrofluid concentration in a qFCS device could lead to a shift in $\phi_{\text{cell-beads}}$ profiles. Figure 4g shows that decreasing the flow ratio (ferrofluid: buffer) resulted in a slightly larger range of $\phi_{
m cell-beads}$ being profiled. Taken together, these data show that the qFCS devices are flexible in profling $\phi_{
m cell-beads}$ with variable combinations of ferrofluid concentrations and flow ratios (ferrofluid: buffer) to suit specific cell types and properties. We observe that the current qFCS device provides excellent multimodal cell isolation in differentiating cell-beads complexes with subtle cellular magnetic contents $\phi_{ ext{cell-beads}}$. Figure 4h summarizes the mean cellular magnetic contents $\phi_{ ext{cell-beads}}$ in each cell-collection chamber of the device from the five cell experiments described above. Each cell-collection chamber of the qFCS device can profile cells with consistent cellular magnetic contents $\phi_{\text{cell-beads}}$ across different cell types (0.28– 0.34 in chamber #1, 0.13-0.15 in chamber #2, 0.09-0.10 in chamber #3, 0.05-0.07 in chamber #4, 0.03-0.05 in chamber #5, 0.02-0.03 in chamber #6, and 0.005-0.01 at the waste outlet). We summarize the ranges of cellular magnetic contents $\phi_{
m cell-beads}$ in each cell-collection chamber in Table 1, which shows that the simulation and experimental data obtained from the qFCS calibration in Figure 3 are consistent with each other.

Next we evaluated qFCS ability in profiling the density of antigen-binding capacity $\alpha_{\rm S}$ for cells and compared it to flow cytometry. We know that cellular magnetic content $\phi_{ ext{cell}- ext{beads}}$ is proportional to $\alpha_{\rm S}/D_{\rm cell}$ from eq 7. As a result, once the cellular magnetic content $\phi_{
m cell-beads}$ and cellular diameter $D_{
m cell}$ are experimentally determined, we can use them to calculate α_s . Because k in eq 2 was unknown in this experiment, we chose to profile cells based on the density of $n_{\text{magnetic-beads}}$, which is proportional to α_s . For experiments, we first conducted a flow cytometry measurement for ~1,000,000 PMBCs that were fluorescently labeled with an antibody targeting anti-CD45. After flow cytometry analyses, fluorescent intensities of ~10,000 cells from this experiment are summarized and plotted (Figure 4i, inset). We note that the flow cytometry requires a relatively large number of target cells for antigen profiling. In contrast to flow cytometry, the qFCS device provided accurate profiling of antigen-binding capacity densities even with only ~1,000 target cells. These ~1,000 PMBCs in the qFCS experiment were indirectly labeled with magnetic beads (diameter: 1.05 μ m; magnetic content: 11.5% (v/v)) that use the same antibody targeting the same antigen

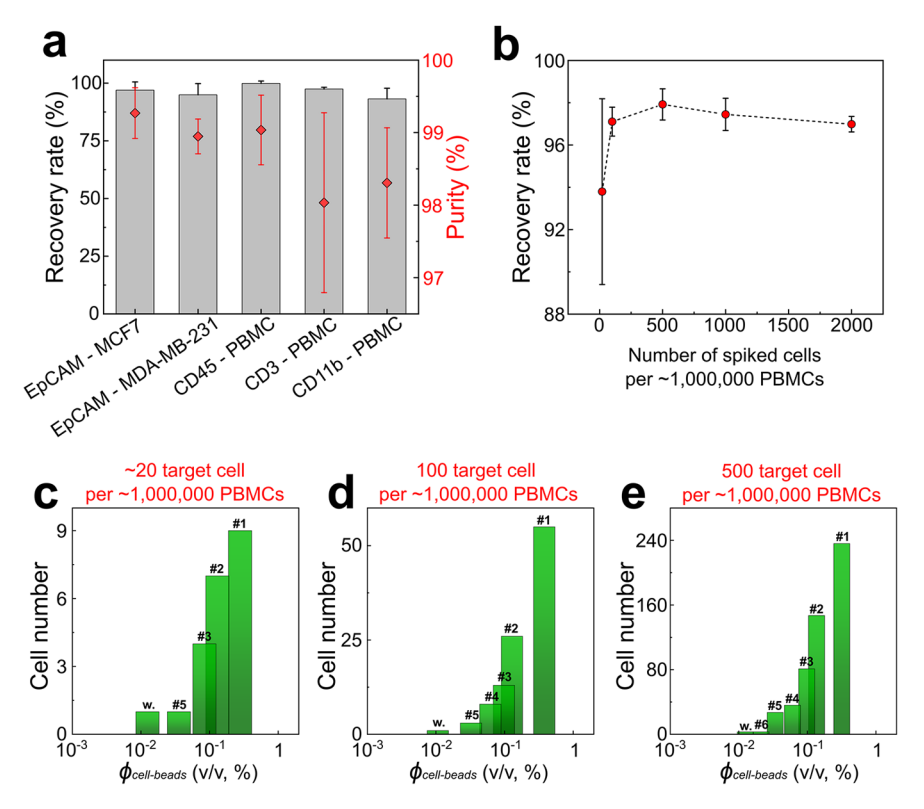


Figure 5. Experimental validation of the qFCS device for its capabilities of isolating rare cells. (a) Recovery rates and purities of spiked cells. Recovery rate of 96.96 \pm 3.59%, 94.95 \pm 4.87%, 99.90 \pm 1.01%, 97.45 \pm 0.76%, and 93.18 \pm 4.63% were achieved for MCF7 targeting EpCAM, MDA-MB-231 targeting EpCAM, PBMCs targeting CD45, PBMCs targeting CD3, and PBMCs targeting CD11b, respectively (all values are mean \pm s.d., n = 3). Purities of 99.27 \pm 0.35%, 98.95 \pm 0.24%, 99.03 \pm 0.48%, 98.03 \pm 1.24%, and 98.31 \pm 0.76% were achieved for MCF7 targeting EpCAM, MDA-MB-231 targeting EpCAM, PBMCs targeting CD45, PBMCs targeting CD3, and PBMCs targeting CD11b, respectively (all values are mean \pm s.d., n = 3). (b) Relationship between the cell recovery rate and the number of spiked cells. A series of cell spike-in experiments were conducted to quantity the recovery rate of the qFCS device in recovering low-concentration cells. A certain number (20, 100, 500, 1,000, and 2,000) of PBMCs indirectly labeled with magnetic beads targeting CD3 were spiked into ~1,000,000 unlabeled PBMCs and processed by qFCS devices. Recovery rates of 93.78 \pm 4.39%, 97.11 \pm 0.68%, 97.92 \pm 0.74%, 97.44 \pm 0.76%, and 96.98 \pm 0.37% were achieved for 20, 100, 500, 1,000, and 2,000 spiked cells, respectively (all values are mean \pm s.d., n = 3). (c-e) Quantifying antigen binding of CD3 among PBMCs with the qFCS devices at extremely low target cell frequencies. (c) ~20, (d) 100, and (e) 500 human white blood cells (WBCs) labeled with CD3-modified magnetic beads. These labeled cells were spiked into ~1,000,000 unlabeled PBMCs with a final volume of 200 μ L and then processed by the qFCS devices. qFCS device processing parameters included a starting ferrofluid concentration ϕ ferrofluid of 0.15% (v/v), a ferrofluid flow rate of 5 μ L min⁻¹, and a buffer flow rate of 50 μ L min⁻¹. Isolated cells in the chambers of the qFCS device were counted and calculated for their cellular magnetic contents ϕ cell-be

as in the flow cytometry experiments (anti-CD45). Before qFCS processing, these cells were first imaged and analyzed for both cellular magnetic contents $\phi_{ ext{cell-beads}}$ and cellular diameters D_{cell} and showed a similar antigen-binding capacity density profile to the flow cytometry (Figure 4i). Labeled cells were spiked into ~1,000,000 unlabeled PBMCs with a final volume of 200 μ L, then processed by a qFCS device. Cells in each cell-collection chamber of the device were analyzed again for their antigen-binding capacity densities. Figure 4j shows that after qFCS processing qFCS returned a similar profile of overall cellular antigen-binding capacity density to the one in Figure 4i. Figure 4j also shows that the cells separated into different cell-collection chambers possessed distinct bead densities which are proportional to antigen-binding capacity densities, confirming qFCS' ability to profile and separate cells based on antigen binding (Figure 4k). In summary, through the experimental determination of cellular magnetic content $\phi_{
m cell-beads}$ in qFCS, together with the determination of cellular diameter D_{cell} from imaging analysis, we can profile cells according to their antigen-binding capacity in three scenarios (Figure 41): (1) cell profiling based on a "cell volumetric

antigen-binding capacity" $\alpha/D_{\rm cell}^3$; (2) cell profiling based on the ratio of antigen-binding capacity density to cellular diameter $\alpha_{\rm S}/D_{\rm cell}$; (3) cell profiling based on antigen-binding capacity α alone when cellular diameters are constant.

Cell Isolation by qFCS. We next evaluated the qFCS device in its ability to isolate rare cells based on their antigen bindings among a cell population. We assessed the performance of qFCS in the cancer cell and PBMC isolation, including the cell recovery rate and purity at extremely low target cell frequencies. For a total of five cell and antigen types, qFCS showed close-to-complete recovery rates across all five experiments (96.96 \pm 3.59%, 94.95 \pm 4.87%, 99.90 \pm 1.01%, $97.45 \pm 0.76\%$, and $93.18 \pm 4.63\%$ for MCF7 targeting EpCAM, MDA-MB-231 targeting EpCAM, PBMCs targeting CD45, PBMCs targeting CD3, and PBMCs targeting CD11b, mean \pm s.d., n = 3 for each experiment) (Figure 5a). Purities of recovered cells are 99.27 \pm 0.35%, 98.95 \pm 0.24%, 99.03 \pm 0.48%, $98.03 \pm 1.24\%$, and $98.31 \pm 0.76\%$ for MCF7 targeting EpCAM, MDA-MB-231 targeting EpCAM, PBMCs targeting CD45, PBMCs targeting CD3, and PBMCs targeting CD11b, respectively (all values are mean \pm s.d., n = 3). The mean

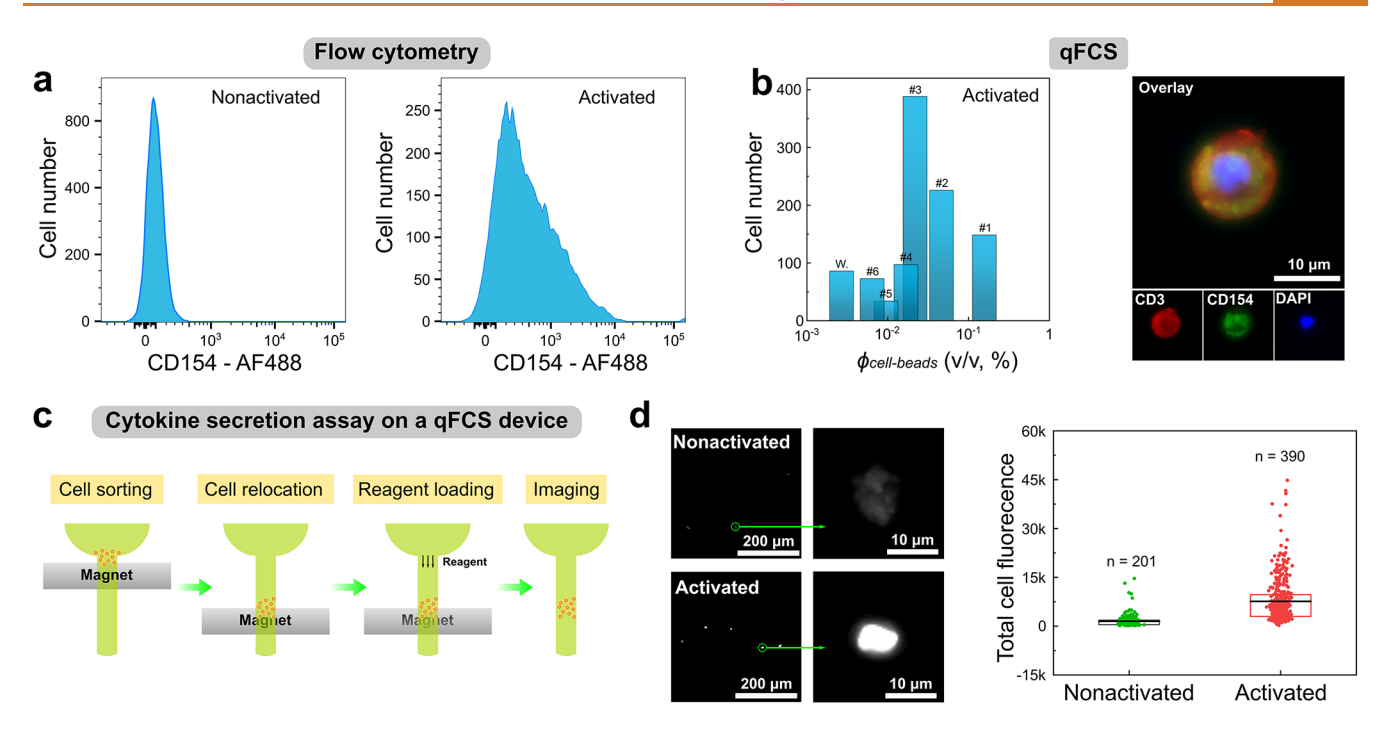


Figure 6. Quantifying and isolating T lymphocytes based on the antigen binding of a low-expression CD154. (a) Quantification of CD154 antigen expressions of ~10,000 nonactivated (left panel) and activated (right panel) T lymphocytes using flow cytometry. (b) (Left panel) Quantification of CD154 expressions of ~1,000 activated T lymphocytes in a qFCS device. About 1,000 cells labeled with CD154-modified magnetic beads were spiked into ~1,000,000 PBMCs and suspended in a 200 μ L ferrofluid. qFCS processing conditions included a starting ferrofluid concentration $\phi_{\text{ferrofluid}}$ of 0.03% (v/v), a ferrofluid flow rate of 5 μ L min⁻¹, and a buffer flow rate of 50 μ L min⁻¹. (Right panel) Fluorescent image of an activated T lymphocyte. After qFCS processing, isolated T lymphocytes were immunofluorescently stained with anti-CD3 (AF647), anti-CD154 (AF488), and nucleic marker (DAPI). (c) Procedure of T lymphocyte cytokine secretion assay. After qFCS processing, isolated cells were relocated toward the collection outlet by moving the permanent magnet. Reagents were then loaded into the collection outlet while the cells were trapped by the magnet. Cells were incubated on the device and imaged. (d) Fluorescence images of nonactivated (top panel) and activated (bottom panel) T lymphocytes. T lymphocytes were incubated with reagents designed to capture their secreted cytokine (IL2). Activated T lymphocytes were collected from cell-collection chamber #3 of the qFCS device. Fluorescence intensities of T lymphocytes labeled with IL-2 capture reagent. The mean cell fluorescence intensities were 1,502 \pm 1,934 (mean \pm s.d., n = 201) for the nonactivated cells and 7,623 \pm 6,722 (mean \pm s.d., n = 390) for the activated cells.

recovery rate across all experiments is 96.49%, and the mean purity of recovered cells across all experiments is 98.72%. We further challenged the qFCS device with low-frequency cell spiking to evaluate its ability to recover rare cells, in which a controlled number (20, 100, 500, 1,000, and 2,000) of PBMCs indirectly labeled with magnetic beads targeting CD3 were spiked into ~1,000,000 unlabeled PBMCs (lowest target to background cells frequency: 1:50,000) and processed by qFCS devices. Close-to-complete recovery rates of 93.78 \pm 4.39%, $97.11 \pm 0.68\%$, $97.92 \pm 0.74\%$, $97.44 \pm 0.76\%$, and $96.98 \pm$ 0.37% were achieved for 20, 100, 500, 1,000, and 2,000 spiked cells, respectively (all values are mean \pm s.d., n = 3). The profiling ability of qFCS was also evaluated at these extremely low target cell frequencies, as shown in Figure 5c-e. Even at the lowest target to background cell frequency of 1:50,000, where ~20 PBMCs indirectly labeled with magnetic beads targeting CD3 were spiked into ~1,000,000 unlabeled PBMCs, qFCS still returned accurate cellular magnetic content profiles like the ones in higher target cell frequencies.

We evaluated the biocompatibility of the qFCS method by first measuring the viabilities of cells expressing CD3 before and after the qFCS processing, whose values were determined to be 93.7 \pm 2.2% (mean \pm s.d., n = 3) and 91.8 \pm 1.6% (mean \pm s.d., n = 3), respectively (Supporting Information Figure S13), showing a negligible impact on cell viability from the qFCS processing. We also measured the long-term prolifer-

ation of isolated cells expressing CD3 from a qFCS device. After a 30-day expansion, flow cytometry data show that isolated cells have lower carboxyfluorescein succinimidyl ester (CFSE) intensity due to the cell proliferation compared to a control group, confirming that isolated cells retain their proliferation function. Taken together, these experimental data show that the qFCS method can simultaneously profile antigen-binding capacities and isolate rare cells based on their antigen-binding capacities in a multimodal and biocompatible manner

Simultaneous Profiling and Isolating Rare Cells Based on a Low-Expression Antigen. We further evaluated the qFCS device for its ability to simultaneously profile and isolate T lymphocytes based on the binding of a low-expression surface antigen molecule: CD154. CD154, also known as CD40 ligand, is a member of the tumor necrosis factor (TNF) family and a type II transmembrane protein predominantly expressed on activated CD4 T lymphocytes.³⁶ Because of its potent effects in both humoral and cell-mediated immunity, dysregulation of CD154 expression has been found in autoimmune diseases. Quantification of the CD154 expression and isolation of cells according to their CD154 levels for downstream analyses become important in diagnosing and understanding autoimmune diseases. However, lower surface expression of CD154 is a well-known challenge that makes it difficult to accurately profile CD154 expression and isolate

cells that express CD154. We applied the qFCS devices to profile and isolate T lymphocytes that express CD154 among PBMCs at a low target cell frequency. We first measured the expression of CD154 on activated T lymphocytes with flow cytometry. Figure 6a shows that the majority of ~10,000 activated T lymphocytes have lower expression levels of CD154. As a result, we optimized the qFCS operating parameter by choosing a low starting ferrofluid concentration of 0.03% (v/v), which allowed us to profile and isolate T lymphocytes with low-expression CD154. T lymphocytes used in this experiment were first activated and treated with CD40 antibody with a commercial kit to prevent the loss of transiently upregulated CD154. These activated T lymphocytes were indirectly labeled with biotinylated anti-CD154 magnetic beads (diameter: 1.05 μ m; magnetic content: 11.5% (v/v)). About 1,000 labeled T lymphocytes were spiked into \sim 1,000,000 unlabeled PBMCs with a final volume of 200 μ L and then processed using a qFCS device. Figure 6b shows that the qFCS device not only returned a CD154 binding profile at the single-cell resolution that resembled flow cytometry but also recovered CD154+ T lymphocytes with a recovery rate of 91.84% and a purity of 99.17%. Recovered CD154+ T lymphocytes from the qFCS device were confirmed for their identity via immunofluorescence (CD3+/CD154+/DAPI+) in Figure 6b. We also studied the impact on the T lymphocytes from the qFCS processing through a cytokine secretion assay that was performed entirely within the qFCS device (Figure 6c). In this assay, isolated CD154+ cells within the cellcollection chambers of the qFCS device were relocated and held by the permanent magnet to allow for their on-device cytokine secretion assay. Figure 6d shows that the isolated CD154+ cells have increased secretion of IL-2 compared to the nonactivated cells, confirming that qFCS can isolate T lymphocytes with a low-expression CD154 on their surface while maintaining their important cellular functions.

CONCLUSIONS

Multimodal sorting of rare cells based on the levels of a specific surface antigen while at the same time quantifying the binding capacity of that antigen is essential in understanding and treating diseases. Unfortunately, conventional methods, including FACS and MACS, did not meet this need, as they either need a large number of target cells or their output is bimodal. Recognizing the need, we developed a microfluidic method, termed quantitative ferrohydrodynamic cell separation, that achieved multimodal rare cell sorting and simultaneous antigen profiling via cellular magnetic content of magnetically labeled cells, which correlates to the cell's antigen-binding capacity. We exploited this correlation in a prototype qFCS device that offers characterization and isolation of magnetically labeled rare cells with single-cell resolution according to their antigen-binding capacity.

Even though magnetism-based cell separation methods have been demonstrated in the past, none of them used a combination of both cellular "diamagnetophoresis" and "magnetophoresis" in biocompatible ferrofluids for cell applications. The integration of these two magnetic manipulation mechanisms in one qFCS device enabled us to simultaneously measure a single cell's intrinsic antigen-binding capacity through magnetic labeling and manipulate the labeled cell into one of the cell-collection chambers according to its antigen-binding capacity for further analysis. To understand the benefit of qFCS over other existing methods, we surveyed a

total 11 magnetism-based cell profiling and/or separation methods and compared their performance to the qFCS (Supporting Information Table S1).^{4,16-26} qFCS and its device have the following advantages over existing methods, including recently published magnetic ratcheting, 16 magnetic ranking cytometry, ¹⁷ cell tracking velocimetry, ¹⁹ and magneto-phoretic cytometer. ¹⁸ First, qFCS not only profiles cells' antigen-binding capacities but also sorts and recovers cells in a biocompatible manner for both on-device and downstream analyses, while other methods including magnetic ranking cytometry, cell tracking velocimetry, and magnetophoretic cytometry only provide antigen-profiling capabilities. 17-19 Second, qFCS offers better overall performance in the multimodal separation of cells with a mean 96.49% recovery of rare cells and a 98.72% purity of recovered cells compared to existing methods. 16-19 Third, qFCS has a high level of sensitivity and is able to profile and isolate rare cells accurately when they are present at down to 1:50,000 target to background cell frequency, while only one of the existing methods-magnetic ranking cytometry-can offer a competing level of sensitivity. 17 Lastly, qFCS is versatile in that it can profile and isolate cells even when the antigen expressions are extremely low. qFCS allows users to adjust the starting ferrofluid concentration and the flow ratio so that the range of the antigen-binding capacity profiling can be varied to suit specific cell types and properties.

The current qFCS device has its own limitations that need to be addressed in future development. First, the current qFCS device has a limited number of stages and cell-collection chambers, which makes its cell profiling coarse when compared to conventional methods such as FACS. Increasing the number of stages and cell-collection chambers for qFCS is not trivial, as it involves a delicate balance of sample flow and device complexity. Second, the current gFCS device is suitable for processing a limited number of cells due to its relatively slow flow rate. Increasing its flow rate and cell-processing throughput would require a redesign of the overall device architecture. Third, when used for cell profiling, qFCS relies on information including both cellular magnetic contents and cellular diameters in order to quantify cells' antigen-binding capacity. This requires additional imaging and analysis of cells after qFCS processing. Future generations of qFCS should consider developing on-device cell diameter measurement to automate the quantification of antigen-binding capacity.

METHODS/EXPERIMENTAL

Modeling and Simulation. Flow profiles and ferrofluid concentrations in the qFCS device were simulated and optimized using COMSOL Multiphysics version 5.5 (COMSOL Inc., Stockholm, Sweden). Creeping flow and transport of diluted species modules were used in the COMSOL studies to simulate flow profiles and distributions of ferrofluid concentration in the qFCS device. Ferrofluid properties, including the density of the ferrofluid of 1,030–1,060 kg/cm³, the viscosity of ferrofluid of 0.99–1.68 mPa·s, and mean diameter of maghemite nanoparticles of 11.2 nm, were used in these studies. Flow rates of the ferrofluid and the PBS buffer were 1–10 μ L/min and 10–100 μ L/min, respectively. Initial concentration of the ferrofluid was 0.03–0.3% (v/v).

Magnetic fields, cell trajectories, and the cell isolation process in the qFCS device were simulated in MATLAB (MathWorks, Natick, MA, USA) using a previously published physical model. ^{31,37–39} Briefly, this three-dimensional model simulates the transport of magnetizable cells in a ferrofluid inside a microfluidic channel coupled with permanent magnets. This model uses the combination of an analytical solution of magnetic field distribution and experimentally verified ferrofluid

magnetization together to calculate magnetic forces on cells. The balance of magnetic force and hydrodynamic drag force on cells in low-Reynolds-number flow condition is then used to simulate the cell trajectories. Parametric studies of device geometries/dimensions, magnetic field distributions, and operating parameters including ferrofluid concentration and flow rates can be conducted in MATLAB using this model. Ferrofluid concentration values can be obtained from previous COMSOL simulations. Details of the model can be found in the Supporting Information.

Microfluidic Device Fabrication. The mold of the qFCS device was fabricated using an SU-8 2025 photoresist (Kayaku Advance Materials, Westborough, MA, USA) with a height of \sim 50 μ m. Microfluidic devices were fabricated using polydimethylsiloxane (PDMS) following standard soft lithography procedures. The fabricated microfluidic device was placed on a 3D-printed manifold to be integrated with one NdFeB permanent magnet (N52, K&J Magnetics, Pipersville, PA, USA). The permanent magnet had a geometry of 50.8 mm \times 6.35 mm \times 6.35 mm ($L \times W \times H$) and a measured remnant magnetization of 1.48 T.

Ferrofluid Synthesis and Characterization. The water-based biocompatible ferrofluid was synthesized by a chemical coprecipitation method following a developed protocol. 40,41 Size and morphologies of the maghemite nanoparticles in the ferrofluid were characterized using a transmission electron microscope (TEM; FEI, Eindhoven, The Netherlands). The diameter of magnetic nanoparticles was measured to be 10.91 ± 4.86 nm. Magnetic properties, including saturation magnetization (1,107 A m⁻¹) and volume fraction of magnetic contents (0.298%, v/v) of the as-synthesized ferrofluid, were obtained through fitting to the Langevin function with data measured using a vibrating sample magnetometer (VSM, MicroSense, Lowell, MA, USA). The viscosity of the as-synthesized ferrofluid was measured to be 1.7 mPa·s using a compact rheometer (Anton Paar, Ashland, VA, USA).

Cell Culture. Cancer Cell Lines. Human breast cancer cell lines, MCF-7 and MDA-MB-231 (ATCC, Manassas, VA, USA), were cultured in the DMEM medium (Thermo Fisher Scientific, Waltham, MA, USA) supplemented with 10% (v/v) fetal bovine serum (Thermo Fisher Scientific), 0.1 mM nonessential amino acids solution (NEAA, Thermo Fisher Scientific), and 1% (v/v) penicillin/streptomycin solution (Thermo Fisher Scientific). Cultured cells were harvested through incubation with 0.05% trypsin-EDTA (Thermo Fisher Scientific) at 37 °C for 3 to 5 min. The concentration of cells was measured with an automated cell counter (Countess, Thermo Fisher Scientific).

Peripheral Blood Mononuclear Cells. Human buffy coat blood was purchased from a commercial vendor (Zen-Bio, Research Triangle, NC, USA) and diluted with an equal volume of noncomplemented DMEM medium. To obtain PBMCs from the blood sample, 20 mL of Ficoll-Paque PLUS (Cytiva, Marlborough, MA, USA) was added to the bottom of a 50 mL conical tube; then 30 mL of diluted blood was loaded into the tube. The tube was centrifuged at room temperature at 760g for 20 min with the brakes off. PBMCs were harvested between the Ficoll and plasma layer and washed three times with PBS by centrifugation at 350g for 8 min. The concentration of PBMCs was measured by the automated cell counter and adjusted to 1×10^6 cells mL⁻¹. PBMCs were cultured in 24-well plates (37 °C, 5% CO₂) at a density of $(1-10) \times 10^6$ cells mL⁻¹ using RPMI-1640 medium (Thermo Fisher Scientific) supplemented with 10% (v/v) fetal bovine serum (FBS), 0.1 mM NEAA solution, and 1% (v/v) penicillin/streptomycin solution.

Cell Labeling. *Magnetic Bead Preparation.* Streptavidin-coated magnetic beads (Dynabeads, Thermo Fisher Scientific) used in this study have a physical diameter of 1.05 μ m. The volume fraction of magnetic material in the beads was determined to be 11.5%. The magnetic beads were first washed with 0.01% Tween 20 solution (Alfa Aesar, Haverhill, MA, USA), followed by blocking with 0.1% bovine serum albumin (BSA, Thermo Fisher Scientific) in PBS solution. Biotinylated primary antibodies, including anti-EpCAM (Miltenyi Biotec, Bergisch Gladbach, Germany), anti-CD3 (Miltenyi Biotec), anti-CD45 (eBioscience, San Diego, CA, USA), anti-CD11b

(eBioscience), and anti-CD154 (Biolegend, San Diego, CA, USA) were first diluted to a concentration of 0.1 mg mL⁻¹. The beads were then precoated with the biotinylated primary antibodies at room temperature for 30 min and then washed twice with PBS before use.

Cell Preparation. Harvested cells were mixed with biotinylated primary antibody-coated magnetic beads for 30 min at room temperature. The labeled cells with ≥1 beads were captured using a magnet system (DynaMag, Thermo Fisher Scientific) and washed with PBS. The number of labeled cells was confirmed with a Nageotte counting chamber (Hausser Scientific, Horsham, PA, USA). In cell tracking experiments, labeled cells were stained with CellTracker Green (Thermo Fisher Scientific), and background cells (unlabeled PBMCs) were stained with CellTracker Orange (Thermo Fisher Scientific) to track their trajectories. Cells were mixed with the ferrofluid before use.

qFCS Experiment Procedure. qFCS devices were first treated with air plasma for 3 min, followed by 70% (v/v) ethanol flushing for 10 min to render the channel surface hydrophilic. The microchannel of the qFCS devices was then primed to reduce nonspecific binding using PBS supplemented with 0.5% (w/v) BSA and 2 mM EDTA (Thermo Fisher Scientific). The microchannel was flushed with PBS for 10 min to remove debris before sample loading. Cell-collection outlets of the qFCS devices were blocked with 3D-printed pillars during isolation experiments. Sample fluids (ferrofluid and cells) and buffer fluids (PBS) were individually controlled with a syringe pump (Chemyx, Stafford, TX, USA) at variable flow rates during the experiments. After qFCS processing, images of cells in the qFCS device's cell-collection chambers were obtained using an inverted microscope equipped with a CCD camera (Carl Zeiss, Germany). Images of cells were analyzed by the ImageJ software to extract the cell's diameter. The effective diameter of the cells was calculated using their surface areas with the assumption that cells were spherical. The number of magnetic beads on each cell was counted and used to calculate cellular magnetic contents for individual cells.

Cell Recovery Rate and Purity Calculations. Cells were counted from both the cell-collection chambers and the waste outlet after a qFCS cell isolation experiment. Cells with CellTracker green fluorescent signal were identified as the target cells, while cells with CellTracker fluorescent orange signal were identified as the background cells. The recovery rate of target cells in a qFCS experiment was calculated by $n_{\text{target-cell-chambers}}/(n_{\text{target-cell-chambers}} + n_{\text{target-cell-waste}})$, where $n_{\text{target-cell-chambers}}$ is the number of target cells in all six cell-collection chambers and $n_{\text{target-cell-chambers}}$ is the target cells in a qFCS experiment was calculated as $n_{\text{target-cell-chambers}}/(n_{\text{target-cell-chambers}} + n_{\text{background-cell-chambers}})$, where $n_{\text{background-cell-chambers}}$ is the number of background cells in all six cell-collection chambers.

Flow Cytometry. The expression levels of antigens were profiled using a flow cytometer (Agilent Quanteon, Agilent, Santa Clara, CA, USA). In a typical flow cytometry experiment, cells were first blocked with UltraCruz Blocking Reagent (Santa Cruz Biotechnology, Dallas, TX, USA) at 4 °C for 20 min. Cells were then suspended in PBS solution supplemented with 2% BSA, 2 mM EDTA, and 2 mM NaN₃ (Sigma-Aldrich, St. Louis, MO, USA). Antibodies with fluorophore were spiked into PBS solution with a volume ratio of 1:50 and incubated with the cells on ice for 30 min, then washed twice and resuspended in cold PBS prior to the flow cytometry. A control group with unlabeled cells was used to set the gate.

T Lymphocytes Activation Assay. PBMCs were cultured in a 24-well plate at a density of 1×10^7 cells mL⁻¹. To activate the T lymphocytes, $20~\mu\text{L}$ of CytoStim reagent (Miltenyi Biotec) and $10~\mu\text{L}$ of CD40 ($1~\mu\text{g}~\text{mL}^{-1}$, Miltenyi Biotec) were added, mixed, and incubated with 10^7 PBMCs at 37 °C for 4 h. Cells were mixed with cold isolation buffer (AutoMACS rinsing solution, Miltenyi Biotec) supplemented with 5% BSA, centrifuged at 300g for 10 min to remove the supernatant, and resuspended with $100~\mu\text{L}$ of cold isolation buffer. Biotinylated anti-human CD154 (Miltenyi Biotec) was conjugated with magnetic beads, and the biotinylated anti-CD154 coated magnetic beads were added into the cell suspension with a volume ratio of 1:30 and incubated for 30 min at room temperature. Labeled

cells were harvested using the DynaMag and resuspended with an isolation buffer. The exact cell number was determined using a Nageotte counting chamber.

On-Device Cytokine Secretion Assay. After processing with qFCS, anti-CD154-labeled cells were directed into the incubation chamber by moving the permanent magnet toward the cell-collection outlets and flushed with warm FBS-free cell culture medium. The device was placed in a cell incubator (37 °C, 5% CO₂) for 20 min. The IL-2 secretion assay was performed using a cell enrichment and detection kit (Miltenyi Biotec). Briefly, the IL-2 catch reagent was infused into the device and incubated for 50 min to allow IL-2 secretion and capture. Cells were then washed with cold buffer (PBS supplemented with 0.5% BSA and 2 mM EDTA) to remove extra reagent. IL-2 detection antibody was infused into the cell-collection chamber and incubated with the cells for 10 min on ice. The chambers were washed with cold buffer and imaged. A control group was prepared with nonactivated cells.

On-Device Immunofluorescence Staining. After processing with qFCS, the medium in the cell-collection chambers was replaced with PBS. The isolated cells were fixed with 4% (w/v) paraformaldehyde solution (PFA, Santa Cruz Biotechnology) for 10 min and subsequently permeabilized with 0.1% (v/v) Triton X-100 (Alfa Aesar) for 10 min. UltraCruz blocking reagent was applied to the cells for 30 min at room temperature to reduce nonspecific bindings. After blocking, cells were immunostained with primary antibodies, including anti-CD154-Alexa Fluor 488 (eBioscience) and anti-CD3-Alexa Fluor 647 (Santa Cruz Biotechnology). After overnight immunofluorescence staining, cells were washed and stained with DAPI (Electron Microscopy Sciences, Hatfield, PA, USA) for imaging.

Cell Viability and Proliferation Assay. Live/Dead Assay. Isolated cells in the cell-collection chambers were washed with Dulbecco's phosphate-buffered saline (D-PBS, Thermo Fisher Scientific) to remove the ferrofluid. Cells were then incubated in the chambers with D-PBS buffer containing 2 μ M Calcein AM and 4 μ M EthD-1 for 30 min at room temperature. After the incubation, cells were washed with D-PBS to remove extra reagents and imaged.

Proliferation Assay. Isolated cells in the cell-collection chambers were collected and placed in a 24-well plate. A 0.5 mL amount of PBS supplemented with 5 μ M CellTrace CFSE staining solution (Thermo Fisher Scientific) was added to each well, and the cells were incubated at 37 °C for 20 min. A 1 mL amount of warm OpTmizer T cell Expansion SFM (Thermo Fisher Scientific), supplemented with 2 mM L-glutamine (Thermo Fisher Scientific) and 150 IU mL⁻¹ (Thermo Fisher Scientific), was then added to each well and incubated for an additional 5 min. Cells were centrifuged (5 min, 300g) and resuspended with OpTmizer T cell Expansion SFM. Cells were stimulated with 1 μ g mL⁻¹ CD3 and 1 μ g mL⁻¹ CD28 on day 1 and restimulated every 7 days. A control group was prepared using cells without CD3 and CD28 stimulation. On day 30, cells were harvested and analyzed for CellTrace CFSE signals with the flow cytometer (Agilent Quanteon, Agilent).

ASSOCIATED CONTENT

5 Supporting Information

The Supporting Information is available free of charge at https://pubs.acs.org/doi/10.1021/acsnano.2c04542.

Derivation of equations to relate cellular magnetic content of a cell—bead complex to its surface antigen-binding capacity, derivation of magnetic forces on the cell—beads complex and the effect of beads' interaction on the magnetic force calculation, relationship between light absorbance of a ferrofluid and its concentration (volume fraction of magnetic materials), governing equations for cell trajectory in qFCS, simulation and experimental data on the ferrofluid concentration in qFCS devices at constant flow ratios (ferrofluid: buffer), magnetic flux density and gradient of flux density in the

qFCS device, simulation data on the ferrofluid concentration profiles at variable starting ferrofluid concentrations across six cell-collection chambers in the qFCS device, simulation data on maximum flow rates for qFCS, simulation data of cell—beads complexes corresponding to Figure 3b (left panel) in the main text, cellular diameter distribution across six qFCS cell-collection chambers, cellular diameter distribution within six qFCS cell-collection chambers, biocompatibility of the qFCS processing, comparison of qFCS to competing technologies (PDF)

AUTHOR INFORMATION

Corresponding Authors

Yang Liu — Department of Chemistry, The University of Georgia, Athens, Georgia 30602, United States; Email: yl63930@berkeley.edu

Leidong Mao — School of Electrical and Computer
Engineering, College of Engineering, The University of
Georgia, Athens, Georgia 30602, United States;
orcid.org/0000-0001-9473-5590; Email: mao@uga.edu

Author

Rafaela Maggioni Simoes Vieira – J. Crayton Pruitt Family Department of Biomedical Engineering, The University of Florida, Gainesville, Florida 32611, United States

Complete contact information is available at: https://pubs.acs.org/10.1021/acsnano.2c04542

Author Contributions

L.M. conceived the idea of the quantitative ferrohydrodynamic cell separation and supervised the research. Y.L. designed the qFCS device and its research and performed the experiments. L.M. and Y.L. analyzed the data. R.V. contributed to the modeling and simulation through the support from a research experience for undergraduates (REU) program. Y.L. and L.M. wrote the manuscript with inputs from all authors.

Notes

The authors declare the following competing financial interest(s): The quantitative ferrohydrodynamic cell separation (qFCS) technology is the subject of the United States utility patent application. Intellectual property related to the qFCS is owned by the University of Georgia Research Foundation. Leidong Mao and Yang Liu are the inventors of the qFCS. Leidong Mao founded and owned FCS Technology LLC with an intent to commercialize qFCS. Leidong Mao has a financial interest in FCS Technology LLC, which is subject to certain restrictions under the university policy. The terms of this arrangement are being managed by the University of Georgia in accordance with its conflict of interest policies.

ACKNOWLEDGMENTS

We thank the Cytometry Shared Resource Laboratory at the Center for Tropical and Emerging Global Diseases at the University of Georgia for their assistance in the flow cytometry analysis. This material is based upon work supported by the National Science Foundation under Grant Nos. 1150042, 1659525, and 1648035; the National Center for Advancing Translational Sciences of the National Institutes of Health under Award No. UL1TR002378, and the National Institute of Biomedical Imaging and Bioengineering of the National Institutes of Health under Award No. 1R41EB028191-01.

The content is solely the responsibility of the authors and does not necessarily represent the official views of the National Institutes of Health.

REFERENCES

- (1) Labib, M.; Wang, Z. J.; Ahmed, S. U.; Mohamadi, R. M.; Duong, B.; Green, B.; Sargent, E. H.; Kelley, S. O. Tracking the Expression of Therapeutic Protein Targets in Rare Cells by Antibody-Mediated Nanoparticle Labelling and Magnetic Sorting. *Nat. Biomed Eng.* **2021**, 5 (1), 41–52.
- (2) Ozkumur, E.; Shah, A. M.; Ciciliano, J. C.; Emmink, B. L.; Miyamoto, D. T.; Brachtel, E.; Yu, M.; Chen, P. I.; Morgan, B.; Trautwein, J.; Kimura, A.; Sengupta, S.; Stott, S. L.; Karabacak, N. M.; Barber, T. A.; Walsh, J. R.; Smith, K.; Spuhler, P. S.; Sullivan, J. P.; Lee, R. J.; et al. Inertial Focusing for Tumor Antigen-Dependent and -Independent Sorting of Rare Circulating Tumor Cells. *Sci. Transl Med.* 2013, 5 (179), 179ra47–179ra47.
- (3) Chen, Y. C.; Li, P.; Huang, P. H.; Xie, Y. L.; Mai, J. D.; Wang, L.; Nguyen, N. T.; Huang, T. J. Rare Cell Isolation and Analysis in Microfluidics. *Lab Chip* **2014**, *14* (4), 626–645.
- (4) Poudineh, M.; Aldridge, P.; Ahmed, S.; Green, B. J.; Kermanshah, L.; Nguyen, V.; Tu, C.; Mohamadi, R. M.; Nam, R. K.; Hansen, A.; Sridhar, S. S.; Finelli, A.; Fleshner, N. E.; Joshua, A. M.; Sargent, E. H.; Kelley, S. O. Tracking the Dynamics of Circulating Tumour Cell Phenotypes Using Nanoparticle-Mediated Magnetic Ranking. *Nat. Nanotechnol* **2017**, *12* (3), 274–281.
- (5) Singh, M.; Jackson, K. J. L.; Wang, J. J.; Schofield, P.; Field, M. A.; Koppstein, D.; Peters, T. J.; Burnett, D. L.; Rizzetto, S.; Nevoltris, D.; Masle-Farquhar, E.; Faulks, M. L.; Russell, A.; Gokal, D.; Hanioka, A.; Horikawa, K.; Colella, A. D.; Chataway, T. K.; Blackburn, J.; Mercer, T. R.; Langley, D. B.; et al. Lymphoma Driver Mutations in the Pathogenic Evolution of an Iconic Human Autoantibody. *Cell* **2020**, *180* (5), 878–894.
- (6) McCutcheon, M.; Wehner, N.; Wensky, A.; Kushner, M.; Doan, S.; Hsiao, L.; Calabresi, P.; Ha, T.; Tran, T. V.; Tate, K. M.; Winkelhake, J.; Spack, E. G. A Sensitive Elispot Assay to Detect Low-Frequency Human T Lymphocytes. *J. Immunol Methods* **1997**, 210 (2), 149–166.
- (7) Raddassi, K.; Kent, S. C.; Yang, J. B.; Bourcier, K.; Bradshaw, E. M.; Seyfert-Margolis, V.; Nepom, G. T.; Kwok, W. W.; Hafler, D. A. Increased Frequencies of Myelin Oligodendrocyte Glycoprotein/Mhc Class Ii-Binding Cd4 Cells in Patients with Multiple Sclerosis. *J. Immunol* 2011, 187 (2), 1039–1046.
- (8) Poudineh, M.; Sargent, E. H.; Pantel, K.; Kelley, S. O. Profiling Circulating Tumour Cells and Other Biomarkers of Invasive Cancers. *Nat. Biomed Eng.* **2018**, *2* (2), 72–84.
- (9) Alix-Panabieres, C.; Pantel, K. Clinical Prospects of Liquid Biopsies. *Nat. Biomed Eng.* **2017**, *1* (4), 1–3.
- (10) Massague, J.; Obenauf, A. C. Metastatic Colonization by Circulating Tumour Cells. *Nature* **2016**, 529 (7586), 298–306.
- (11) Krebs, M. G.; Metcalf, R. L.; Carter, L.; Brady, G.; Blackhall, F. H.; Dive, C. Molecular Analysis of Circulating Tumour Cells-Biology and Biomarkers. *Nat. Rev. Clin Oncol* **2014**, *11* (3), 129–44.
- (12) Heitzer, E.; Haque, I. S.; Roberts, C. E. S.; Speicher, M. R. Current and Future Perspectives of Liquid Biopsies in Genomics-Driven Oncology. *Nat. Rev. Genet* **2019**, *20* (2), 71–88.
- (13) Ma, N.; Jeffrey, S. S. Deciphering Cancer Clues from Blood. Science 2020, 367 (6485), 1424–1425.
- (14) Givan, A. L. Principles of Flow Cytometry: An Overview. *Method Cell Biol.* **2001**, *63*, 19–50.
- (15) Miltenyi, S.; Muller, W.; Weichel, W.; Radbruch, A. High-Gradient Magnetic Cell-Separation with Macs. *Cytometry* **1990**, *11* (2), 231–238.
- (16) Murray, C.; Miwa, H.; Dhar, M.; Park, D. E.; Pao, E.; Martinez, J.; Kaanumale, S.; Loghin, E.; Graf, J.; Raddassi, K.; Kwok, W. W.; Hafler, D.; Puleo, C.; Di Carlo, D. Unsupervised Capture and Profiling of Rare Immune Cells Using Multi-Directional Magnetic

- Ratcheting (Vol 18, Pg 2396, 2018). Lab Chip 2018, 18 (23), 3703-3703.
- (17) Labib, M.; Philpott, D. N.; Wang, Z. J.; Nemr, C.; Chen, J. B.; Sargent, E. H.; Kelley, S. O. Magnetic Ranking Cytometry: Profiling Rare Cells at the Single-Cell Level. *Acc. Chem. Res.* **2020**, *53* (8), 1445–1457.
- (18) Civelekoglu, O.; Liu, R. X.; Usanmaz, C. F.; Chu, C. H.; Boya, M.; Ozkaya-Ahmadov, T.; Arifuzzman, A. K. M.; Wang, N. Q.; Sarioglu, A. F. Electronic Measurement of Cell Antigen Expression in Whole Blood. *Lab Chip* **2022**, *22* (2), 296–312.
- (19) McCloskey, K. E.; Moore, L. R.; Hoyos, M.; Rodriguez, A.; Chalmers, J. J.; Zborowski, M. Magnetophoretic Cell Sorting Is a Function of Antibody Binding Capacity. *Biotechnol. Prog.* **2003**, *19* (3), 899–907.
- (20) Sutermaster, B. A.; Darling, E. M.Considerations for High-Yield, High-Throughput Cell Enrichment: Fluorescence Versus Magnetic Sorting. *Sci. Rep-Uk***2019**, *9*, DOI: 10.1038/s41598-018-36698-1.
- (21) Schneider, T.; Karl, S.; Moore, L. R.; Chalmers, J. J.; Williams, P. S.; Zborowski, M. Sequential Cd34 Cell Fractionation by Magnetophoresis in a Magnetic Dipole Flow Sorter. *Analyst* **2010**, 135 (1), 62–70.
- (22) Reisbeck, M.; Helou, M. J.; Richter, L.; Kappes, B.; Friedrich, O.; Hayden, O. Magnetic Fingerprints of Rolling Cells for Quantitative Flow Cytometry in Whole Blood. *Sci. Rep-Uk* **2016**, 6 (1), 1–11.
- (23) Yenilmez, B.; Knowlton, S.; Tasoglu, S. Self-Contained Handheld Magnetic Platform for Point of Care Cytometry in Biological Samples. *Adv. Mater. Technol-Us* **2016**, *1* (9), 1600144.
- (24) Liu, Y.; Zhao, W. J.; Cheng, R.; Puig, A.; Hodgson, J.; Egan, M.; Pope, C. N. C.; Nikolinakos, P. G.; Mao, L. D. Label-Free Inertial-Ferrohydrodynamic Cell Separation with High Throughput and Resolution. *Lab Chip* **2021**, *21* (14), 2738–2750.
- (25) Kose, A. R.; Koser, H. Ferrofluid Mediated Nanocytometry. Lab Chip 2012, 12 (1), 190–196.
- (26) Chen, Q.; Li, D.; Zielinski, J.; Kozubowski, L.; Lin, J. H.; Wang, M. H.; Xuan, X. C. Yeast Cell Fractionation by Morphology in Dilute Ferrofluids. *Biomicrofluidics* **2017**, *11* (6), 064102.
- (27) Gijs, M. A. M.; Lacharme, F.; Lehmann, U. Microfluidic Applications of Magnetic Particles for Biological Analysis and Catalysis. *Chem. Rev.* **2010**, *110* (3), 1518–1563.
- (28) McCloskey, K. E.; Chalmers, J. J.; Zborowski, M. Magnetophoretic Mobilities Correlate to Antibody Binding Capacities. *Cytometry* **2000**, *40* (4), 307–315.
- (29) McCloskey, K. E.; Comella, K.; Chalmers, J. J.; Margel, S.; Zborowski, M. Mobility Measurements of Immunomagnetically Labeled Cells Allow Quantitation of Secondary Antibody Binding Amplification. *Biotechnol. Bioeng.* **2001**, *75* (6), 642–655.
- (30) Rosensweig, R. E. Ferrohydrodynamics; Cambridge University Press: Cambridge, 1985.
- (31) Zhao, W.; Liu, Y.; Jenkins, B. D.; Cheng, R.; Harris, B. N.; Zhang, W.; Xie, J.; Murrow, J. R.; Hodgson, J.; Egan, M.; Bankey, A.; Nikolinakos, P. G.; Ali, H. Y.; Meichner, K.; Newman, L. A.; Davis, M. B.; Mao, L. Tumor Antigen-Independent and Cell Size Variation-Inclusive Enrichment of Viable Circulating Tumor Cells. *Lab Chip* **2019**, *19* (10), 1860–1876.
- (32) Liu, Y.; Zhao, W. J.; Cheng, R.; Harris, B. N.; Murrow, J. R.; Hodgson, J.; Egan, M.; Bankey, A.; Nikolinakos, P. G.; Laver, T.; Meichner, K.; Mao, L. D. Fundamentals of Integrated Ferrohydrodynamic Cell Separation in Circulating Tumor Cell Isolation. *Lab Chip* **2021**, *21* (9), 1706–1723.
- (33) Liu, Y.; Zhao, W. J.; Cheng, R.; Hodgson, J.; Egan, M.; Pope, C. N. C.; Nikolinakos, P. G.; Mao, L. D. Simultaneous Biochemical and Functional Phenotyping of Single Circulating Tumor Cells Using Ultrahigh Throughput and Recovery Microfluidic Devices. *Lab Chip* **2021**, *21* (18), 3583–3597.
- (34) Zhao, W.; Cheng, R.; Miller, J. R.; Mao, L. Label-Free Microfluidic Manipulation of Particles and Cells in Magnetic Liquids. *Adv. Funct Mater.* **2016**, *26* (22), 3916–3932.

- (35) Zhao, W. J.; Liu, Y.; Jenkins, B. D.; Cheng, R.; Harris, B. N.; Zhang, W. Z.; Xie, J.; Murrow, J. R.; Hodgson, J.; Egan, M.; Bankey, A.; Nikolinakos, P. G.; Ali, H. Y.; Meichner, K.; Newman, L. A.; Davis, M. B.; Mao, L. D. Tumor Antigen-Independent and Cell Size Variation-Inclusive Enrichment of Viable Circulating Tumor Cells. *Lab Chip* **2019**, *19* (10), 1860–1876.
- (36) VanKooten, C.; Banchereau, J. Cd40-Cd40 Ligand: A Multifunctional Receptor-Ligand Pair. *Adv. Immunol* 1996, 61, 1–77. (37) Liu, Y.; Zhao, W.; Cheng, R.; Harris, B. N.; Murrow, J. R.; Hodgson, J.; Egan, M.; Bankey, A.; Nikolinakos, P. G.; Laver, T.; Meichner, K.; Mao, L. Fundamentals of Integrated Ferrohydrodynamic Cell Separation in Circulating Tumor Cell Isolation. *Lab Chip* 2021, 21 (9), 1706–1723.
- (38) Cheng, R.; Zhu, T.; Mao, L. Three-Dimensional and Analytical Modeling of Microfluidic Particle Transport in Magnetic Fluids. *Microfluid. Nanofluid.* **2014**, *16* (6), 1143–1154.
- (39) Zhu, T.; Lichlyter, D. J.; Haidekker, M. A.; Mao, L. Analytical Model of Microfluidic Transport of Non-Magnetic Particles in Ferrofluids under the Influence of a Permanent Magnet. *Microfluid. Nanofluid.* 2011, 10 (6), 1233–1245.
- (40) Zhao, W. J.; Cheng, R.; Lim, S. H.; Miller, J. R.; Zhang, W. Z.; Tang, W.; Xie, J.; Mao, L. D. Biocompatible and Label-Free Separation of Cancer Cells from Cell Culture Lines from White Blood Cells in Ferrofluids. *Lab Chip* **2017**, *17* (13), 2243–2255.
- (41) Liu, Y.; Zhao, W.; Cheng, R.; Logun, M.; Zayas-Viera, M. D. M.; Karumbaiah, L.; Mao, L. Label-Free Ferrohydrodynamic Separation of Exosome-Like Nanoparticles. *Lab Chip* **2020**, *20* (17), 3187–3201.

□ Recommended by ACS

Immunomagnetic Separation Method Integrated with the Strep-Tag II System for Rapid Enrichment and Mild Release of Exosomes

Xiaoniu Guo, Niancai Peng, et al.

JANUARY 20, 2023

ANALYTICAL CHEMISTRY

READ 🗹

Circulating Tumor Cells in Cancer Diagnostics and Prognostics by Single-Molecule and Single-Cell Characterization

Tafsir Chowdhury, Philippe Manivet, et al.

JANUARY 25, 2023

ACS SENSORS

READ 🗹

On-Chip Enrichment System for Digital Bioassay Based on Aqueous Two-Phase System

Yoshihiro Minagawa, Hiroyuki Noji, et al.

DECEMBER 29, 2022

ACS NANO

READ **C**

Graphene as Thinnest Coating on Copper Electrodes in Microbial Methanol Fuel Cells

Jamil Islam, Venkataramana Gadhamshetty, et al.

DECEMBER 19, 2022

ACS NANO

READ 🗹

Get More Suggestions >